1 **Genome-Scale CRISPR Screening Identifies Novel Human Pluripotent Gene**

2 **Networks**

3

4 Robert J. Ihry[1], Max R. Salick[1], Daniel J. Ho[1], Marie Sondey[1], Sravya Kommineni[1], Steven

5 Paula[2], Joe Raymond[1], Elizabeth Frias[2], Kathleen A. Worringer[1], Carsten Russ[2], John Reece-

6 Hoyes[2], Bob Altshuler[1], Ranjit Randhawa[1], Zinger Yang[2], Gregory McAllister[2], Gregory R.

**7** Hoffman[2], Ricardo Dolmetsch[1], and Ajamete Kaykas[1].

8

9 [1]Department of Neuroscience, [2]Department of Chemical Biology and Therapeutics, Novartis

10 Institutes for Biomedical Research, Cambridge, MA 02139, USA

11

12 Corresponding author: Ajamete Kaykas (ajamete.kaykas@novartis.com)

13

14 **ABSTRACT**

15

16 Human pluripotent stem cells (hPSCs) generate a wide variety of disease-relevant cells that can

17 be used to improve the translation of preclinical research. Despite the potential of hPSCs, their

18 use for genetic screening has been limited because of technical challenges. We developed a

19 renewable Cas9/sgRNA-hPSC library where loss-of-function mutations can be induced at will.

20 Our inducible-mutant hPSC library can be used for an unlimited number of genome-wide

21 screens. We screened for novel genes involved in 3 of the fundamental properties of hPSCs:

22 Their ability to self-renew/survive, their capacity to differentiate into somatic cells, and their

23 inability to survive as single-cell clones. We identified a plethora of novel genes with unidentified

24 roles in hPSCs. These results are available as a resource for the community to increase the

25 understanding of both human development and genetics. In the future, our stem cell library

26 approach will be a powerful tool to identify disease-modifying genes.

27

28 **VISUAL ABSTRACT**

1

30

IN BRIEF

31
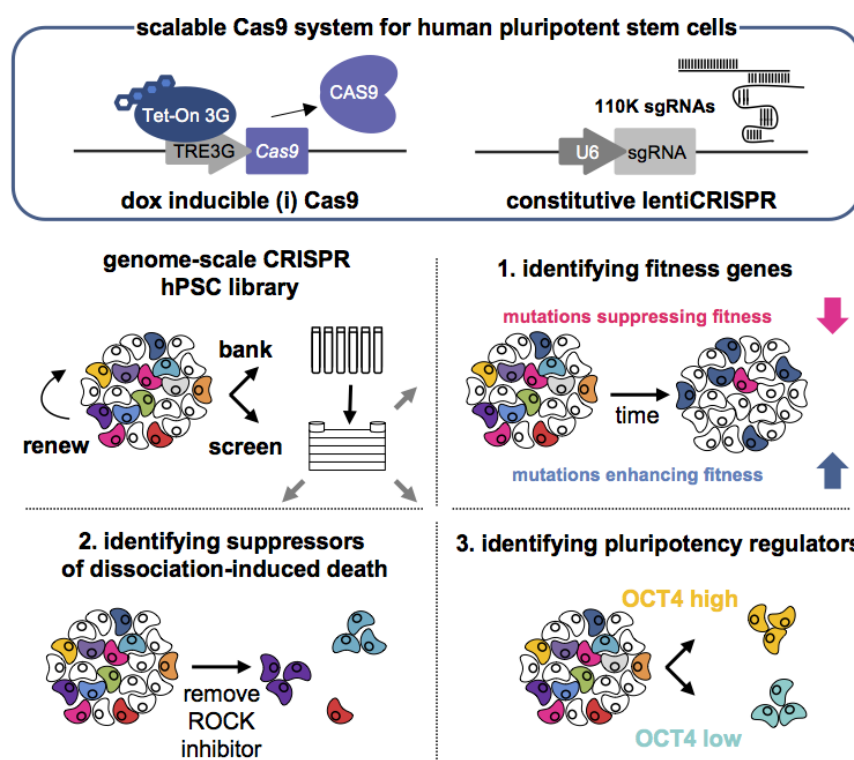
32 Ihry et al. develop a stable CRISPR/Cas9 genetic screening platform tailored for use in hPSCs

33 that enables unbiased genome-scale genetic screening. The platform exhibits high performance

34 at genome-scale and accurately detects the dropout of core essential genes. Furthermore,

35 proof-of-concept screens exploited hPSC-specific phenotypes to identify regulators of fitness,

36 survival after single-cell dissociation, and pluripotency.

HIGHLIGHTS

37

38 ➢ A universal and scalable genetic platform in hPSCs for general use across all lineages

39 ➢ Robust knockout efficiencies translate into high performance screening at genome-scale

40 ➢ Identified stem cell-specific components of *TP53* and *OCT4* genetic networks in hPSCs

41 ➢ Phenotypic screen identifies novel actin/myosin genes regulating membrane blebbing

42 ➢ Identified novel gene sets regulating pluripotency and discovered the roles of *PMAIP1*

43 and *PAWR* in sensitivity to DNA damage and single-cell dissociation

INTRODUCTION

Human pluripotent stem cells (hPSCs) can be used to generate a wide variety of disease relevant cell types and have the potential to improve the translation of preclinical research by enhancing disease models. Despite the huge potential, genetic screening using hPSCs has been limited by their expensive and tedious cell culture requirements (Chen et al., 2011), and reduced genetic manipulation efficiencies (Ihry et al., 2018). Only a few shRNA screens have been conducted in hPSCs (Chia et al., 2010; Zhang et al., 2013), however shRNAs have a high level of off targets and do not cause a complete loss of function, which is difficult to interpret (DasGupta et al., 2005; Echeverri et al., 2006; Kampmann et al., 2015; McDonald et al., 2017). Currently, the CRISPR/Cas9 system is the genetic screening tool of choice because it can efficiently cause loss-of-function alleles (Cong et al., 2013; Jinek et al., 2012; Mali et al., 2013). Hundreds of genome-scale pooled CRISPR screens have been performed in immortalized human cell lines (Hart et al., 2015; Meyers et al., 2017; Wang et al., 2015). However, in hPSCs the CRISPR/Cas9 system has been primarily used for small-scale genome engineering (Merkle et al., 2015). In genetically intact hPSCs the only genome-scale CRISPR screen to date used methods developed for cancer cells, suffered from technical issues, had poor performance, and identified few developmentally relevant genes (Hart et al., 2014; Shalem et al., 2014). We addressed these technical issues by systematically tailoring the CRISPR/Cas9 system for hPSCs (Ihry et al., 2018). We developed a doxycycline (dox) inducible Cas9 (iCas9) hPSC line and stably infected it with a genome-scale sgRNA library. We banked and expanded the CRISPR-infected hPSC library in the absence of editing (-dox), which enabled us to generate a renewable stem cell pool with stable but inactive sgRNAs. This allowed us to conduct multiple independent screens with the same cell library.

In the first screen, we identified genes that suppress or enhance hPSC fitness over long-term culture. While previous screens have generated gold standard gene lists of core essential genes that reduce cell survival when mutated, little is known about the mutations that enhance survival and proliferation. Unlike core essential genes, these enhancing mutations appear to be cell type-specific and no consistent lists exist for this type of gene (Hart et al., 2014). In hPSCs karyotypic analysis has detected recurrent copy number variations (CNVs) that confer a growth advantage (Amps et al., 2011; Laurent et al., 2011); however, these studies lack gene level resolution. Recently, next-generation sequencing of hundreds of hPSCs identified the recurrence of dominant-negative *TP53* mutations that can expand within a population of hPSCs (Merkle et al., 2017). We mined our data for gene knockouts that enriched in culture and identified many genes, including components of the *TP53* pathway and other known tumor

3

78   suppressors. We validated the strongest hit, *PMAIP1/NOXA*, which appears to be a stem cell-
79   specific gene conferring sensitivity to DNA damage downstream of *TP53*.

80   In the second screen, we identified genes required for single-cell cloning. hPSCs have a
81   poor survival rate after dissociation to single-cells, which is detrimental for genome engineering.
82   Multiple groups have extensively characterized death induced by single-cell cloning and have
83   demonstrated the process is similar to but distinct from anoikis and is triggered by a
84   ROCK/Myosin/Actin pathway (Chen et al., 2010; Ohgushi et al., 2010). To prevent death,
85   hPSCs are passaged as clumps or treated with ROCK inhibitors (Watanabe et al., 2007). By
86   subjecting our hPSC mutant library to single-cell dissociation without ROCK inhibitors, we
87   selected for mutations that survive single-cell cloning. sgRNAs for the ROCK and myosin
88   pathways were enriched in the surviving clones. The most enriched gene was the pro-apoptotic
89   regulator *PAWR* (Burikhanov et al., 2009). Validation studies confirmed a novel role for *PAWR*
90   as a component of the actin-cytoskeleton that induces membrane blebbing and cell death
91   caused by single-cell cloning. The additional novel genes identified here will further our
92   understanding about the sensitivity of hPSCs to single-cell cloning.

93   In the final screen, we utilized a FACS-based OCT4 assay to identify regulators of
94   pluripotency and differentiation. Pluripotency is a defining feature of hPSCs and it allows them
95   to differentiate into all three germ layers. *OCT4/POU5F1*, *NANOG* and *SOX2* are critical
96   transcription factors that maintain pluripotency *in vivo* and *in vitro* (Chambers et al., 2007; Masui
97   et al., 2007; Nichols et al., 1998). *OCT4* and *SOX2* overexpression is commonly used to
98   reprogram somatic cells towards the pluripotent state (Takahashi and Yamanaka, 2006;
99   Takahashi et al., 2007; Yu et al., 2007). By isolating mutant cells with high or low OCT4 protein
100   expression we identified many genes involved in maintaining the pluripotent state along with
101   genes involved with induction of differentiation. Overall these lists of genes provide unique
102   insights into the genetic regulation of human development that could only be identified in normal
103   diploid cells that are not transformed or cancerous.

104   By using a doxycycline inducible Cas9 (iCas9) hPSC line stably infected with a genome-
105   scale lentiCRISPR library, we were able to bank a CRISPR-hPSC library that was renewable
106   and enabled a high number of independent screens with the same starting library. This allows
107   direct comparison between screens and reduces screen to screen variability. We rigorously
108   tested the system and identified genes important for fitness, pluripotency, and single-cell cloning
109   of hPSCs. Herein we provide a resource with detailed methods and all available data including
110   many novel genes that are involved in hPSC biology. This resource will serve as a parts list of
111   genes that are functionally important for the human stem cell state. Furthermore, the gene sets

4

112   and methods will increase our systematic knowledge of human pluripotent stem cell biology and

113   will enable additional large-scale CRISPR screens in stem cells and their somatic derivatives.

RESULTS

iCas9 system is a self-renewing resource enabling successive genome-wide genetic screens in hPSCs

We set out to develop a high-throughput CRISPR/Cas9 platform for hPSCs which would enable successive rounds of screening from a stable library of lentiCRISPR-infected hPSCs (Fig. 1A, S1). Generating a genome-scale lentiCRISPR hPSC library would enable both the rigorous testing of CRISPR screen performance and the identification of cell type-specific regulators of the pluripotent state. In our previous work, we developed an all-in-one doxycycline (dox) inducible Cas9 (iCas9) transgene that was inactive in the absence of dox (Ihry et al., 2018). The tight control over Cas9 expression allowed us to transduce cells with lentiviruses expressing sgRNAs (lentiCRISPRs) in the absence of dox without causing on-target indels. We tested if it was possible to bank a genome-scale lentiCRISPR infected cell library (5 sgRNAs per gene, 110,000 total sgRNAs) prior to Cas9 mutagenesis (- dox). After one freeze-thaw cycle, NGS analysis revealed no bottlenecking of the library demonstrating the feasibility of banking a large lentiCRISPR hPSC library for repeated screens (Fig. 1B).

Evaluating the performance of CRISPR screening in iCas9 hPSCs

Next, we performed a fitness screen to evaluate the global performance of the system (Fig. 1C). We benchmarked the performance of the screen by utilizing annotated lists of core essential genes. Core essential genes are required for the survival of all cells; the corresponding CRISPR knockout causes the sgRNAs to be depleted (Hart et al., 2014, 2015). Genome-scale CRISPR screening in hPSCs has been challenging (Hart et al., 2014; Shalem et al., 2014). hPSCs have a strong DNA damage response (DDR) and Cas9-induced double strand breaks (DSBs) cause a significant cell loss (Ihry et al., 2018). Failure to account for Cas9-induced cell loss is problematic for pooled screening because it is critical to maintain representation of each sgRNA-barcoded cell. Our previous work demonstrated a range of Cas9-induced cells loss between 3 to 10-fold across many sgRNAs (Ihry et al., 2018). To prevent bottlenecking of the sgRNA library we conducted the screen in hPSCs at an average of 1000 cells per sgRNA (a total of 110 million infected cells). By doing this we maintained about 4-fold more cells than a typical cancer screen (Hart et al., 2015). During the fitness screen, DNA was sampled before and after dox exposure at days 0, 8, 14, and 18 (Fig. S1). To provide a qualitative measurement of screen performance, we plotted the p-values calculated by the redundant siRNA activity (RSA) test against Q1 based z-scores for a set of core essential and non-essential genes (Hart et al., 2014; König et al., 2007). Before dox treatment the non-essential and core essential genes are randomly distributed within a tight cluster (Fig. 1D). After

148   18 days of Cas9 treatment the distribution spreads and the essential genes significantly dropout

149   while the non-essential genes remain constant (Fig. 1D, File S1-2).

150   To quantify performance, we employed the Bayesian Analysis of Gene EssentiaLity

151   (BAGEL) algorithm which calculates a Bayes factor for each gene by determining the probability

152   that the observed fold change for a given gene matches that of known essential genes (Hart

153   and Moffat, 2016).This generates a ranked list of Bayes factors for each gene, which can then

154   be used to quantify screen performance by precision versus recall analysis. In a high-

155   performance screen, essential genes have high Bayes factor scores and the precision versus

156   recall curve gradually drops off as analysis of the ranked list is completed. In contrast, a poor

157   performing screen has a precision versus recall curve that rapidly drops off, indicating many

158   false positives (non-essential genes) with high Bayes factor scores. The sample without dox

159   exposure (untreated) has a randomly ranked Bayes factor list with non-essential and essential

160   genes interspersed and exhibits a poor precision versus recall curve (Fig. 1E). In the day 18

161   Cas9 (+dox) treated samples, essential genes and non-essential genes segregate from each

162   other and generates a high-performing precision versus recall curve that gradually drops off

163   (Fig. 1E, File S3).

164   After 18 days of Cas9 exposure, we identified 770 fitness genes at a 5% false discovery

165   rate based on of the precision calculation (Fig. 1F, File S4). Comparing the set of 770 hPSC

166   fitness genes to 1580 core essential genes from cancer lines revealed an overlap of 405 genes

167   (Fig. 1G) (Hart et al., 2015). The remaining 365 specifically dropped out in hPSCs. Both the

168   core and hPSC-specific essential genes are abundantly expressed in hPSCs, further supporting

169   that they are required to maintain hPSCs in culture (Fig. 1H). Our fitness screen in hPSCs

170   correctly identifies the dropout of core-essential genes with accuracy that is on par with CRISPR

171   screens conducted in cancer cell lines. This demonstrates that cancer cells and stem cells

172   share a common set of core essential genes that can be used to benchmark performance. By

173   properly accounting for cell loss caused by Cas9 activity, we have overcome a significant

174   technical barrier that has thwarted previous attempts at genome-scale screening in hPSCs (Hart

175   et al., 2014; Shalem et al., 2014). This demonstrates it is possible to conduct an effective

176   genome-scale CRISPR screen in hPSCs using the methods described here.

177   ***TP53* pathway mutations specifically enrich during CRISPR fitness screen in hPSCs**

178   Curated lists of genes that enhance fitness during a CRISPR screen do not exist,

179   making it difficult to benchmark the enrichment results (Hart et. al., 2015). By comparing the top

180   ~1000 depleted (RSA-down< -2.25, Files S2) and enriched (RSA-up < -2.25, File S5) genes we

181   observed that 31.8% (301 of 946) of the enriched genes were located on the X and Y

182   chromosomes (H1-hESCs XY, Fig. S3). In contrast, the depleted genes were evenly distributed

183   across all chromosomes. It became apparent that allosome targeting sgRNAs were behaving

184   similarly to non-targeting controls which enrich during a CRISPR screen in hPSCs (Ihry et al.,

185   2018). We observed that sgRNAs causing a single DSB on the X chromosome are less toxic

186   relative to sgRNAs inducing 2 DSBs at the *MAPT* locus despite being able to efficiently induce

187   indels (Fig. S2). sgRNAs targeting genomic amplifications in cancer cell lines exhibit a strong

188   depletion irrespective of the gene targets (Aguirre et al., 2016; Meyers et al., 2017; Munoz et al.,

189   2016). Unlike cancer cell lines, H1-hESCs with a normal diploid karyotype and are very

190   sensitive to DNA damage making the difference between 1 and 2 DSBs significant. After

191   recognizing that the enrichment of sgRNAs on the X/Y chromosomes was related to DSB

192   sensitivity and copy number differences in male H1-hESCs we focused on autosomal genes. In

193   the remaining list of 645 autosomal genes that were enriched (RSA-up -2.25) we identified 41

194   tumor suppressor genes (Zhao et al., 2016).

195   The second most enriched gene was *TP53,* which confirms the selective pressure

196   imposed by Cas9-induced DSBs in hPSCs during a CRISPR screen (Fig. 2A). Consistent with

197   this *TP53* mutants are able to suppress cell loss induced by Cas9 activity (Ihry et al., 2018).

198   Throughout the 18-day screen, the representation of sgRNAs targeting *TP53* (Chr. 17), the

199   checkpoint kinase, *CHEK2* (Chr. 22)*,* and the proapoptotic regulator, *PMAIP1* (Chr. 18)*,*

200   increased in a time-dependent manner (Fig. 2B). Database mining for associations with *TP53*

201   among the enriched genes identified 20 genes with direct connections to *TP53* (Fig. 2C, File

202   S6). 19 of which are expressed in H1-hESC and are on autosomal chromosomes. Although

203   *EDA2R* is on the X chromosome, it was included because its mRNA increases in response to

204   DNA damage in hPSCs (Ihry et al., 2018). We hypothesized that these genes could include

205   additional regulators responsible for the extreme sensitivity to DNA damage in hPSCs.

206   *PMAIP1* was the most enriched gene in the screen. PMAIP1 has been implicated in

207   *TP53*-dependent cell death and functions by sensitizing cells to apoptosis by antagonizing the

208   anti-apoptotic protein MCL1 at the mitochondria (Kim et al., 2006; Perciavalle et al., 2012;

209   Ploner et al., 2008). *PMAIP1* is highly expressed in hPSCs and its expression marks the

210   pluripotent state (Mallon et al., 2013). We confirmed this by examining *PMAIP1* expression in 2

211   iPSC and 2 hESC lines. Analysis of RNA-seq experiments confirmed that *PMAIP1* was highly

212   expressed during the pluripotent state and drops during neuronal differentiation using the *NGN2*

213   transgene (Fig. 3A). Additionally, GTEx data revealed that *PMAIP1* has a highly restricted

214   expression pattern and is not expressed in most tissues (GTEx Analysis Release V7). Although

215   it has been demonstrated that *PMAIP1* expression is maintained by *OCT4* in testicular germ cell

8

216   tumors (Gutekunst et al., 2013), no functional connection has been made in hPSCs. We tested

217   if *PMAIP1* expression was maintained by the pluripotency network by differentiating cells or

218   knocking out *OCT4*. Under these conditions qPCR detected a significant decrease in *PMAIP1*

219   mRNA (Fig. 3B). In thymocytes, *PMAIP1* mRNA is induced by TP53 (Khandanpour et al.,

220   2013). We knocked out *TP53* in hPSCs but did not detect a reduction in *PMAIP1* mRNA (Fig

221   3B). hPSCs constitutively express high levels of *PMAIP1,* and DNA damage does not increase

222   *PMAIP1* expression, further supporting *PMAIP1* mRNA as pluripotency-dependent and TP53-

223   independent (Ihry et al., 2018).

224   Prior work demonstrated that cancer cell lines have a reduced DNA damage response

225   relative to hPSCs (Ihry et al., 2018). Consistent with this we did not observe an enrichment of

226   *PMAIP1* sgRNAs in 14 independent CRISPR screens conducted in cancer cell lines despite

227   using libraries containing the same *PMAIP1*-targeting sgRNAs (Fig. 3C). This suggested that

228   *PMAIP1* is responsible for making hPSCs sensitive to DNA damage. To test the functional

229   consequences of *PMAIP1* mutations, we knocked out *PMAIP1* in the iCas9 cell line using

230   transient exposure to synthetic crRNAs (Fig. S3). We tested if *PMAIP1* mutants were resistant

231   to DSB-induced death by using lentiCRISPRs to deliver a sgRNA targeting *MAPT,* a neuronal

232   gene not expressed in hPSCs. In the absence of Cas9 (-dox), both control and *PMAIP1* mutant

233   iCas9 cells grow at a similar rate while expressing an sgRNA. In the presence of Cas9 (+dox)

234   and a sgRNA, control cells die while *PMAIP1* mutants are able to survive despite efficient DSB

235   induction (Fig. 3D, S3, S4E). qPCR analysis of the *TP53*-target genes *P21* and *FAS* detected

236   an elevated expression in *PMAIP1* mutants compared to controls (Fig. 3E). Despite having an

237   active *TP53, PMAIP1* mutants survive. This indicates *PMAIP1* is downstream of *TP53* activation

238   and is consistent with its known role as a sensitizer to apoptosis (Ploner et al., 2008). In hPSCs

239   cell death is the predominant response to DNA damage. Unlike *PMAIP1* mutants, *P21* mutants

240   (>80% indels) are unable to suppress DSB-induced toxicity (Fig. S4E), and *P21* sgRNAs did not

241   enrich in H1-hESCs. In contrast, in a genome-scale screen in retinal pigment epithelial cells,

242   where Cas9 activity causes TP53-dependent cell cycle arrest rather than apoptosis, sgRNAs

243   targeting *TP53* and *P21/CDKN1A* were enriched while *PMAIP1* sgRNAs were not (File S5)

244   (Haapaniemi et al., 2017). Overall, these results indicate that *PMAIP1* plays a role in the

245   sensitivity of hPSCs to DNA damage and highlights the ability of genome-scale CRISPR

246   screens to identify cell type-specific genes important for the fitness of pluripotent stem cells.

247   **Genetic screen for suppressors of dissociation-induced death**

248   We next tested our ability to identify phenotypic regulators of human developmental processes.

249   Human PSCs, unlike mouse PSCs, are very sensitive to dissociation and die in the absence of

9

250 ROCK-inhibitors (Ohgushi et al., 2010). During dissociation of hPSCs, Rho and ROCK become

251 activated. This leads to the phosphorylation of myosin, which causes membrane blebbing and

252 cell death. To promote survival, inhibitors that target ROCK (Y-27632/thiazovivn) or myosin

253 (blebbistatin) are used routinely during hPSC passaging (Chen et al., 2010; Watanabe et al.,

254 2007). Very few cells survive dissociation in the absence of ROCK inhibitors. Importantly, this

255 phenotype is developmentally rooted. hPSCs are epiblast-like and cells that fail to incorporate

256 into the polarized epithelium of the epiblast undergo cell death in the embryo (Ohgushi et al.,

257 2010). To gain a deeper understanding of the genes involved, we screened for suppressors of

258 dissociation-induced death.

259 During the day 14 passage of the fitness screen we plated an additional replicate of the

260 genome-scale mutant cell library in the absence of thiazovivin (Fig. 4A, S1). The majority of the

261 cells died during this process and the surviving cells were maintained for two weeks until large

262 colonies were visible, at which point DNA was isolated and sgRNAs sequences were recovered

263 by NGS. We identified 76 genes with 2 or more independent sgRNAs present in cells that

264 survived dissociation without thiazovivin (Fig. 4C and File S7). As expected, multiple sgRNAs

265 targeting *ROCK1* and *MYH9,* the genetic targets of ROCK inhibitors and blebbistatin, were

266 recovered. Myosin is a hexameric motor protein that is comprised of 6 subunits with 3 subtypes.

267 The screen recovered 3 sgRNAs for *MYH9,* a myosin heavy chain, 5 sgRNAs for *MYL6,* a non-

268 phosphorylated myosin light chain, and 2 sgRNAs for the ROCK target *MYL9/MLC2,* a

269 phosphorylated myosin light chain. There are many myosin proteins, but our screen identified 3

270 out of 5 of the most abundantly expressed in hPSCs (Fig. 4B). This reiterates the importance of

271 myosin activation in membrane blebbing and dissociation-induced death. A number of additional

272 genes have roles in the actin/myosin network or cytoskeleton, including *DAPK3, PAWR,*

273 *OPHN1, FLII* and *KIF3A* (Fig. 4D). Overall STRING-DB analysis detected a connected set of

274 genes with ties to the actin/myosin regulatory network (Fig. 4D). In general members of this

275 network did not enrich during the fitness screen suggesting they specifically regulate

276 dissociation-induced death and not fitness (Fig. 4E).

277 **PAWR is required for dissociation-induced death**

278 For follow-up studies, we focused on the strongest hit from the screen, the pro-apoptotic

279 regulator *PAWR* (Hebbar et al., 2012). *PAWR* has no known biological role in the early embryo

280 or during dissociation-induced death of hPSCs. The screen recovered all 5 sgRNAs targeting

281 *PAWR* in the genome-scale library and the barcode reads were highly abundant (Fig. 4C).

282 Unlike sgRNAs for the *TP53* pathway that enrich throughout the CRISPR screen, *PAWR* and

283 *MYL6* have no effect on fitness in the presence of thiazovivin (Fig. 4E). We repeated the results

284   using 3 independent lentiCRISPRs to knock out *PAWR* in iCas9 expressing H1-hESC cells.

285   *PAWR* mutants are able to survive without thiazovivin while control cells do not (Fig. S4). To

286   independently validate these results, we used CRISPR mediated interference (CRISPRi) to

287   knockdown the expression of *PAWR* mRNA without causing DNA damage or genetic mutations

288   (Qi et al., 2013). By using a H1-hESC line constitutively expressing dCas9 fused to a KRAB

289   domain and sgRNAs targeting *PAWR* promoter we also detected an increase in the survival of

290   dissociated cells in the absence of thiazovivin (Fig. S4).

291   To conduct detailed analysis of *PAWR* mutants we exposed cells to Cas9 RNPs

292   targeting *PAWR* and generated a knockout cell line with a normal karyotype (Fig. S4). The

293   suppression of dissociation-induced death is specific to *PAWR* mutants, as *PMAIP1* mutants

294   are unable to survive passaging without thiazovivin (Fig. 5A-B). Conversely, *PAWR* mutants are

295   unable to survive DSB-induced toxicity, further demonstrating the specificity of the respective

296   phenotypes (Fig. S4E). We next examined how *PAWR* mutants survive by time-lapse

297   microscopy. After single cell dissociation, control cells without thiazovivin exhibit membrane

298   blebbing and subsequently die (Fig 5C). Conversely, *PAWR* mutants without thiazovivin have

299   greatly reduced blebbing and survive as single cells by extending cell projections, which

300   promote attachment and survival (Fig 5C). We further examined cytoskeletal organization using

301   phalloidin to stain filamentous (F-) ACTIN. The thiazovivin-treated cells have an increased

302   surface area, a fanned-out shape with actin stress fibers, and a large circular adhesion belt-like

303   structure (Fig. 5C). In the absence of thiazovivin, control cells have many small actin rings which

304   mark membrane blebs. *PAWR* mutants without thiazovivin exhibit reduced membrane blebbing

305   and small actin rings (Fig. 5C).

306   Molecularly, *PAWR* has dual roles as a transcriptional repressor that causes cell death

307   or as an actin binding protein that regulates contractility (Burikhanov et al., 2009; Johnstone et

308   al., 1996; Vetterkind and Morgan, 2009). Despite having abundant *PAWR* mRNA, PAWR

309   protein is post-trancriptionally regulated and induced by dissociation in hPSCs (Fig. S4-5).

310   Immunofluorescence did not detect PAWR protein in the nucleus; however, we did observe

311   localization of PAWR with F-ACTIN in both thiazovivin treated and untreated cells (Fig. 5D).

312   PAWR localized to adhesion belt-like structures in the presence of thiazovivin and to membrane

313   blebs in the untreated cells after dissociation. Additional hits from the screen, PRKCZ and

314   SCRIB, also localized to membrane blebs (Fig. S6). Both PRKCZ and SCRIB are expressed in

315   the early mouse embryo and exhibit a ROCK-dependent cell polarity (Kono et al., 2014).

316   Cumulatively, we have identified a novel role for *PAWR* in dissociation-induced death. *PAWR*

317   mutants survive dissociation without ROCK inhibitors because of a failure to initiate membrane

11

318 blebbing and downstream caspase activation (Fig S5) (Ohgushi et al., 2010). Furthermore,

319 *PAWR* is a known proapoptotic factor and we have demonstrated that PAWR protein is induced

320 upon dissociation and colocalizes with the ACTIN network that is responsible for initiating

321 membrane blebbing and subsequent cell death.

322 **FACS-based screen for regulators of pluripotency**

323   Although our fitness screen detected a significant hPSC-specific dropout of *OCT4* other

324 critical regulators of pluripotency like *NANOG* did not affect fitness (Fig 1E, File S4). A genome

325 scale fitness screen in mouse ESCs had similar results and only reported the dropout of three

326 genes regulating blastocyst development (Koike-Yusa et al., 2014). Pluripotency and cellular

327 fitness of hPSCs may not be related and this indicates that some differentiated cell types may

328 not exhibit changes in fitness when cultured in the pluripotent media. To specifically identify

329 regulators of human pluripotency we conducted a FACS-based pooled screen using an OCT4

330 antibody. One year after conducting the first fitness screen we thawed a genome-scale CRISPR

331 cell library and expanded them prior to conducting the screen (Fig. S1). The cells were

332 mutagenized with Cas9 for 8 days prior to FACS to collect cells with high (OCT4^{HIGH}) and low

333 (OCT4^{LOW}) OCT4 expression (Fig. 6A). Log2(fold change) was calculated by comparing the

334 OCT4^{LOW} group to the OCT4^{HIGH} group. We plotted the p-values calculated by the RSA test

335 against Q1 and Q3 based z-scores for OCT4^{LOW} and OCT4^{HIGH}, respectively (Fig. 7B, File S8).

336 Importantly, we detected a significant enrichment of *OCT4* and *NANOG* targeting sgRNAs in the

337 OCT4^{LOW} group. We also detected an enrichment of *TGFBR1/2* genes required to maintain the

338 culture of hPSCs and the chromatin regulators *EP300* and *SMARCA4/BRG1* which regulate

339 *OCT4* expression and function in hPSCs (Chen et al., 2011; King and Klose, 2017; Singhal et

340 al., 2010; Wang et al., 2012). Using STRING-db we identified a core network of genes

341 connected to *OCT4* in the OCT4^{LOW} group (Fig. 6C). This highlights the ability of phenotypic

342 CRISPR screening to identify relevant gene networks. Additionally, the OCT4^{HIGH} group

343 identified factors that promote differentiation such as *HAND1*, *KDM5B, and EIF4G2*, (File S8)

344 (Hough et al., 2006; Kidder et al., 2013; Yamanaka, 2000). Many of the genes in these lists

345 have published roles in regulating pluripotency, reprogramming or embryonic development, and

346 further investigation of the less studied genes will reveal novel insights into the human

347 pluripotent state (File S8-9).

348 **Identification of hPSCs specific fitness and pluripotency gene networks**

349   Extensive CRISPR screening in cancer cell lines has provided a wealth of knowledge

350 about their genetic dependencies. However, the static state of these cells has revealed less

351 about genes with developmental functions (Hart et al., 2015). To compare hPSC results to

12

352   cancer cell lines we conducted pairwise Pearson correlation coefficients using Bayes factors

353   distributions (cancer data from Hart et al., 2015). The analysis revealed that hPSCs formed a

354   distinct cluster (Fig. 7A) and is consistent with the partial overlap between core essential genes

355   in cancer and fitness genes in hPSCs (52% Fig. 1E). To focus on gene networks specific to

356   hPSCs we conducted bioinformatics analysis comparing 829 core essentials cancer genes

357   (essential for 5/5 cell lines, Hart et al., 2015) to hPSC-specific gene sets identified by our

358   screens. A total of 661 hPSC-specific genes were obtained from the fitness screen (365

359   depleted and 20 enriched p53 related genes), dissociation-induced death screen (76), and the

360   OCT4 FACS screen (212) (File S10). The gene lists were analyzed using the PANTHER

361   classification system (pantherdb.org). PANTHER pathway analysis identified a greater diversity

362   of 92 enriched pathways in hPSCs and only 38 in the cancer lines (Fig. 7B). In accordance with

363   this we also detected an increase in the number of genes with receptor and signal transducer

364   activity molecular functions (Fig. 7C). The hPSC-enriched pathways included several expected

365   regulators: FGF, TGF-Beta, and WNT (Fig. 7B). FGF2 and TGFβ are critical components of E8

366   media and are required to maintain pluripotency *in vitro* (Chen et al., 2011). WNT signaling

367   regulates both differentiation and pluripotency in ESCs (Sokol, 2011). Activation of EGF, PDGF,

368   and VEGF is also important for the maintenance of the pluripotent state in (Fig. 7B) (Brill et al.,

369   2009). P53 and CCKR/Rho GTPases pathways, which regulate apoptosis and have critical roles

370   in determining the sensitivity of hPSCs to DNA damage and enzymatic dissociation, were also

371   enriched (Fig. 7B). Examination of the biological processes gene ontology revealed an increase

372   in the number of development and multicellular organism genes (Fig. 7C). Furthermore, sub-

373   dividing the developmental process category revealed enrichment of genes regulating cell

374   death, differentiation and early developmental stages (Fig. 7C). Globally these results highlight

375   the identification of cell type-specific genes regulating different aspects of the pluripotent state.

376   By screening for regulators of 3 fundamental processes governing the culture of hPSCs we

377   have successfully identified known regulators in addition to a plethora of novel genes involved in

378   stem cell biology (Fig. 7D). These genes are a blueprint for human pluripotency and will serve

379   as a useful resource for the human development and stem cell communities.

380 **DISSCUSSION**

381   The use of hPSCs in large-scale functional genomics studies has been limited by
382 technical constraints. Prior to our study, it was unclear that genome-scale CRISPR screens
383 were possible in hPSCs as the first attempts had poor performance (Hart et al., 2014; Shalem et
384 al., 2014). We overcame this by building a high-performance 2-component CRISPR/CAS9
385 system for hPSCs. The performance, across many sgRNAs, made the platform amenable to
386 high-throughput screening. Using iCas9 in hPSCs it is possible to perturb hundreds of genes in
387 arrayed format or the entire genome in pooled format. The system is renewable and a pool of
388 stem cells with sgRNAs to the entire genome can be banked, distributed and utilized for
389 successive screens in hPSCs and their differentiated progeny. Beyond technical proficiency we
390 identified genes that regulate fundamental stem cell processes such as self-renewal, their
391 inherent sensitivity to DNA damage, single-cell cloning, pluripotency and differentiation.

392   First, we identified 770 genes required for the self-renewal of hPSC. A majority of these
393 genes have established roles in fitness while 365 of these genes are novel and specific to
394 hPSCs. This set of genes could be used to inform a systematic approach to improve the
395 consistency, robustness and user-friendliness of hPSC culture conditions. During the fitness
396 screen, we also determined that Cas9 activity imposes a selective pressure on DNA damage
397 sensitive hPSCs. This caused an enrichment of 20 genes that are connected to *TP53*.
398 Consistent with this, dominant negative *TP53* mutations and deletions recurrently occur and
399 provide a selective advantage during the culture of hPSCs (Amir and Laurent, 2016; Merkle et
400 al., 2017). In addition to *TP53,* we identified a hPSC-specific role for *PMAIP1* in determining the
401 extreme sensitivity of hPSCs to DNA damage. Like *TP53*, deletions of chromosome 18
402 spanning the *PMAIP1* locus have been recurrently observed during hPSC culture (Amps et al.,
403 2011) and suggest that *PMAIP1* deletion may be responsible for enhanced survival of these
404 lines. These *TP53*-related genes have the potential to improve the efficiency or safety of
405 genome engineering through transient inhibition or by monitoring their spontaneous mutation
406 rate during hPSC culture (Ihry et al., 2018; Merkle et al., 2017).

407   Second, we identified 76 genes that enhance the survival of hPSCs during single-cell
408 dissociation. Collectively, the screen uncovered an Actin/Myosin network required for
409 membrane blebbing and cell death caused by dissociation. We identified a novel role for *PAWR*,
410 a pro-apoptotic regulator that is induced upon dissociation. *PAWR* is required for membrane
411 blebbing and subsequent death of dissociated hPSCs in the absence of ROCK inhibitors.
412 Importantly, the results are developmentally relevant, and we also identified *SCRIB* and *PRKCZ*
413 which are known regulators of cell polarity in the early mouse embryo (Kono et al., 2014).

14

414 *PAWR* has been shown to physically interact with *PRKCZ* and suggests a potential link between
415 cell polarity and dissociation-induced death (Díaz-Meco et al., 1996). These hits appear to be
416 related to the polarized epiblast-like state of primed hPSC and could explain why polarized
417 hPSCs are sensitive to dissociation whereas unpolarized naïve mESC are not (Takashima et
418 al., 2015). Lastly, this set of genes could enable focused approaches to improve the single-cell
419 cloning efficiencies of hPSCs and the culture of naïve hPSCs.

420 In the final screen, by subjecting our hPSC CRISPR library to FACS sorting on OCT4
421 protein, we identified 113 genes that are required to maintain pluripotency and 99 genes that
422 potentially regulate differentiation. Overall, the screen identified an entire network of genes
423 related to OCT4. 19 of these genes have previously indicated roles in pluripotency, embryo
424 development and reprogramming (File S9). Future studies on the novel genes in the list will
425 yield new insights about the genetic control of pluripotency and differentiation. These gene sets
426 could guide rational improvements to protocols for the maintenance, differentiation and
427 reprogramming of hPSCs.

428 Overall, the results highlight the ability of unbiased genome-scale screens to identify
429 critical and novel regulators of human pluripotent stem cell biology. Future investigation into the
430 genes provided here will be a step toward the genetic dissection of the human pluripotent state.
431 Herein we provide simple and scalable work flows that will lower the entry barrier for additional
432 labs to conduct large-scale CRISPR screens in hPSCs. The scalable and bankable platform
433 described here is a renewable resource that will allow for successive screens and the
434 distribution of CRISPR infected hPSC libraries. The platform could potentially be used to
435 improve the generation, culture and differentiation capacity of hPSCs. It can be applied to the
436 study of development and disease in wide variety of differentiated cell types. Established
437 protocols for neurons, astrocytes, cardiomyocytes, hepatocytes and beta-cells can be exploited
438 to dissect the genetic nature of development and homeostasis in disease relevant cell types.
439 This resource opens the door for the systematic genetic dissection of disease relevant human
440 cells in way that was only before possible in model organisms.

15

441 **Figure 1: A self-renewing Dox-inducible CAS9/genome-wide sgRNA cell library enables**
442 **multiple high performance CRIPSR screens in human pluripotent stem cells** (A) Diagram
443 depicting the iCas9 platform for genome-scale CRISPR screening in hPSCs. The iCas9 platform
444 consists of a dox-inducible Cas9 transgene knocked in the AAVS1 locus of H1-hESCs and
445 lentiviral delivery of constitutively expressed sgRNAs. iCas9 hPSCs were transduced (.5 MOI)
446 at scale. After a week of expansion and selection for lentiCRISPRs iCas9 hPSCs were either
447 banked or subjected to Cas9 mutagenesis for screening. (B) Correlation of normalized sgRNA
448 counts reveals that freeze/thaw expanded samples (-dox) have high correlation with the plasmid
449 library and the starting pool of infected iCas9 hPSCs at day 0 of the screen. Day 18 samples
450 have been exposed to dox (+Cas9). (C) Diagram depicting three categories of genes that enrich
451 (enhance), deplete (suppress) or remain constant during a fitness screen. (D) Scatter plot
452 depicting gene level results for core essential (pink) and non-essential genes (blue). Without
453 Cas9 treatment (-dox), cells expressing sgRNAs targeting core essential and non-essential
454 genes are interspersed and have an RSA > -2.75 (marked by dashed line). After 18 days of
455 exposure to Cas9 (+dox), sgRNAs targeting essential genes dropout to less than RSA -2.75. Y-
456 axis is RSA value. X-axis marks the Z-score (Q1). Non-essential and core essential gene list
457 from Hart et. al., 2014. (E) Precision v. recall analysis of genome-scale CRISPR screening data
458 in H1-hESCs. Cas9 expressing cells (purple) exhibit a PR curve that gradually slopes off,
459 whereas cells without Cas9 (green) exhibit a PR curve that immediately decreases. (F) Fitness
460 gene calculation based on 5% FDR on y-axis. Each condition labeled on the x-axis. (G) Venn
461 diagram comparing 770 depleted genes in hPSCs to 1580 core essential genes identified by
462 screening cancer cell lines (Hart et. al., 2015). 405 of the hPSCs depleted genes overlap while
463 the remaining 365 are specifically depleted in pluripotent stem cells. (H) Genes that dropout in
464 CRISPR screen are abundantly expressed. Y-axis depicts the $\log_2$ transformation of average
465 TPM values from 20 independent RNA-seq experiments in H1-hESC. For each box blot the
466 median is depicted by white line flanked by a rectangle spanning Q1-Q3. X-axis depicts gene
467 categories. In blue are non-essential genes from Hart et al., 2014, in pink are 405 core-essential
468 genes, in purple are 365 stem cell-specific essential genes and in gray are the remaining
469 unannotated genes.

470 **Figure 1: A renewable lentiCRISPR infected hPSCs library enables high performance**

471 **screeni**

472
473
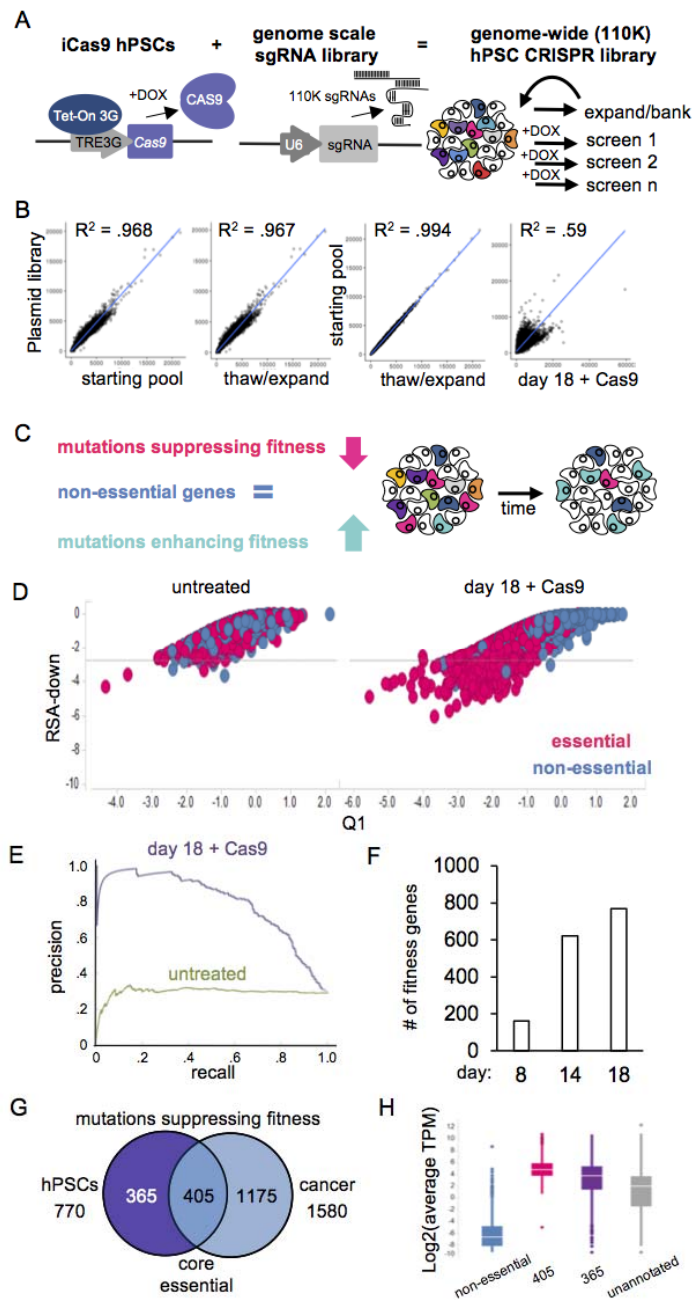
474 **Figure 2: T*P53* pathway mutations enrich during CRISPR screen in hPSCs** (A) Scatter plot
475 depicting gene level results for the genome-scale screen. After 18 days of exposure to Cas9
476 (+dox) sgRNAs targeting *TP53* related genes enrich during the screen; *PMAIP1 (NOXA)* (RSA -
477 10.6, Q3 3.7), *TP53* (RSA -7.64, Q3 4), and *CHEK2* (RSA -3.6, Q3 2.4). A total of 302 genes
478 have a RSA score < -3 (marked by dashed line). *TP53* related genes with RSA scores <-2.25
479 are marked in red. Y-axis is a p-value generated from RSA Up analysis. X-axis marks the Z-
480 score (Q3). (B) Plot showing the time-dependent increase in 5 independent sgRNAs targeting
481 *PMAIP1*, *CHEK2* and *TP53* during CRISPR screen. NGS quantifies representation of
482 lentiCRISPR-infected cells. Samples were normalized to the day 0 population. Y-axis represents
483 log2 (fold change). Day 0 data shown is from freeze/thaw samples. X-axis plots each condition
484 over time. Cas9 + samples were treated with dox to induce Cas9 expression. (C) Shown are
485 gene knockouts (20) that enrich during CRISPR screen that are connected to *TP53* and play
486 roles in either DNA damage response and apoptosis. 946 enriched genes in RSA up < -2.25
487 identified by STRING-DB analysis.

488 **Figure 2: T*P53* pathway mutations enrich during CRISPR screen in hPSCs**

489

490
491
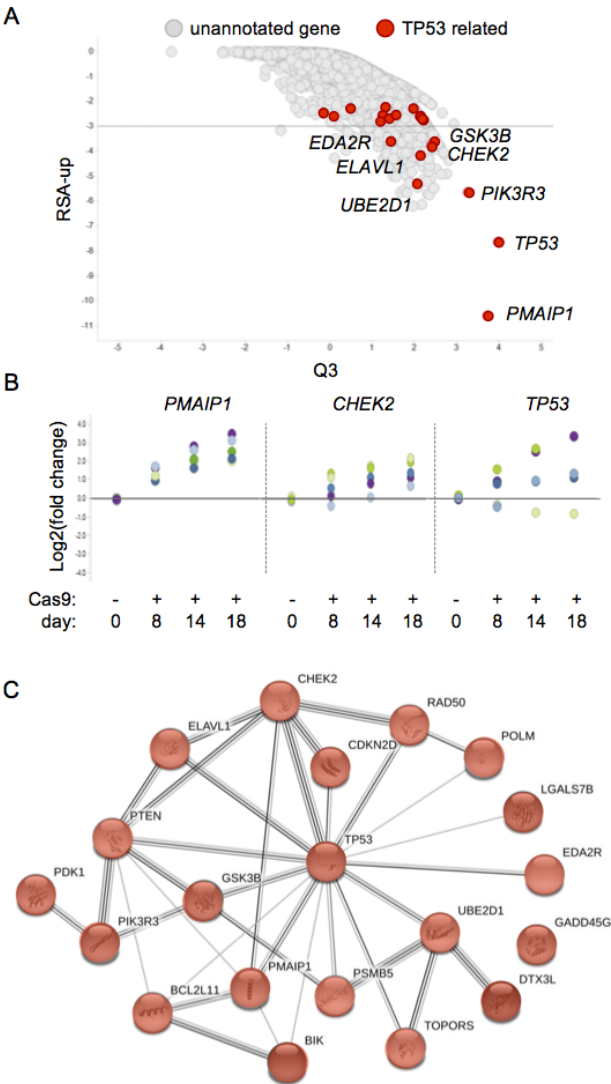
492 **Figure 3: *PMAIP1* confers sensitivity to DNA damage in hPSCs** (A) *PMAIP1* is highly

493 expressed in hESCs and iPSCs. Y-axis represents expression in Transcripts Per Kilobase

494 Million (TPM). H1-hESCs (n=1), H9-hESCs (n=3), 8402-iPSCs (n=3) and HDFn-iPSCs (n=4). X-

495 axis represents days after induction of a doxycycline inducible NGN2 expression cassette. (B)

496 qPCR confirms *PMAIP1* mRNA is dependent on the pluripotent state. Y-axis is relative

497 expression and each bar represents mean relative expression. X-axis is each condition. Control

498 = hPSCs in E8 media, +FBS = 3 days exposure to 10% FBS and DMEM, +NGN2 = 3 days

499 exposure to NGN2, *OCT4* KO = mutant pool after 6 days exposure to iCas9 and sgRNA

500 targeting *OCT4*, PMAIP1-/- = complete knockout cell line, *TP53*-/- = complete knockout cell line.

501 n=3 independent mRNA samples per sgRNA, error bars +/- 1 std. dev. Unpaired two-tailed t-

502 test, equal variances *p<.05, **p<0.01. (C) *PMAIP1* targeting sgRNAs specifically enrich during

503 CRISPR screen in hESC but not cancer cell lines. X-axis plots CRISPR screens conducted in

504 H1-hESC lines and 14 additional transformed lines. 5-independent sgRNAs marked by dots. Y-

505 axis represents log2(fold change). (D) *PMAIP1* mutant hPSCs are insensitive to DNA damage.

506 Live imaging of confluence in *MAPT* sgRNA expressing iCas9 cells +/- DSB (+dox/Cas9) in

507 control or *PMAIP1*$^{-/-}$ knockout cell line. Unlike DSB treated control cells the *PMAIP1*$^{-/-}$ mutants

508 survive in the presence of DSBs. Black lines indicate control and magenta lines indicate

509 *PMAIP1*$^{-/-}$ mutants. Solid lines are without dox and dashed lines are cultured with dox. Y-axis is

510 percent confluency each point represents mean (4 images per well, n=3 wells). error bars +/- 1

511 std. X-axis time in days of treatment. (E) qPCR of *TP53* target genes indicates *PMAIP1*

512 functions downstream of *TP53*. *P21 and FAS* mRNA is induced by *MAPT* targeting sgRNAs in

513 iCas9 control cells 2 days after dox treatment. *PMAIP1*$^{-/-}$ mutants exhibit increased levels of *P21*

514 and *FAS* mRNA which is absent in *TP53*$^{-/-}$ mutants. Y-axis is relative expression is calculated by

515 comparing the *MAPT* targeting sgRNA plus (+dox) or minus Cas9 expression (-dox). Unpaired

516 two-tailed t-test, equal variances *p<.05, **p<0.01, ***p<0.001, ****p<0.0001.

20

517   **Figure 3: *PMAIP1* confers sensitivity to DNA damage in hPSCs**

518
519

520 **Figure 4: Genetic screen for suppressors of dissociation-induced death** (A) Diagram
521 depicting screen shows the dissociation and replating of the genome-scale mutant cell library
522 without the thiazovivin (ROCK inhibitor). Most cells did not survive the treatment; however, at
523 the end of two weeks some large colonies were recovered for DNA isolation and NGS analysis.
524 (B) The screen recovered 3 out of 6 subunits of the hexameric MYOSIN motor protein that
525 regulates blebbing in hPSCs. Y-axis average TPM in H1-hESC. X-axis myosin genes expressed
526 >1 TPM in H1-hESCs. Myosin genes recovered by screen in pink. Genes that were not detected
527 by screen in blue. (C) Heat map depicting number of sgRNAs recovered on y-axis and each
528 gene on x-axis. Colors indicate the abundance of each sgRNA recovered. Pink marks greater
529 than 90 percentile and purple marks less than 10th percentile. (D) String-DB analysis highlights
530 ACTIN and MYOSIN gene network among mutations that allow cells to survive dissociation in
531 the absence of ROCK inhibitors. Hits from screen marked in green. (E) *MYL6* and *PAWR*
532 specifically regulate survival after dissociation and do not enrich during CRISPR screen. Each
533 dot represents 5 independent sgRNAs per gene and NGS quantifies representation of
534 lentiCRISPRs infected cells. Samples were normalized to the day 0 population and y-axis
535 represents log2(fold change). Day 0 data shown is from freeze/thaw samples maintained at
536 2100x. X-axis plots each condition over time. Cas9 + samples were treated with dox to induce
537 Cas9 expression.

538 **Figure 4: Genetic screen for suppressors of dissociation-induced death**
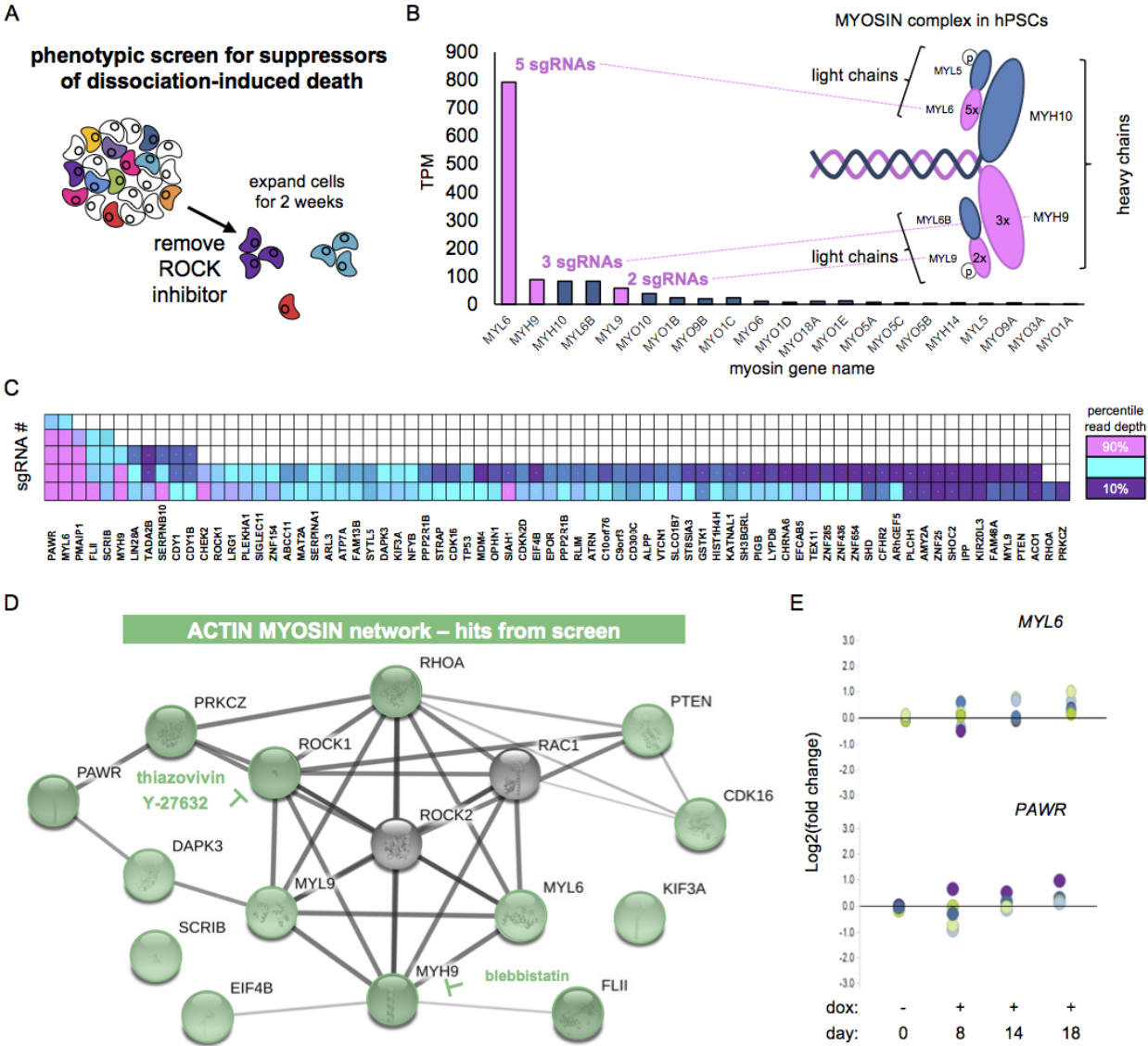
541 **Figure 5: *PAWR* is required for dissociation-induced death** (A) *PAWR* mutants survive

542 single-cell dissociation in the absence of thiazovivin (ROCK inhibitor) treatment. Control cells

543 and *PMAIP1* knockout do not survive without thiazovivin treatment. Bright-field images taken of

544 live iCas9 cells 4 days after dissociation. Scale bar = 800 uM (B) Quantification of survival in the

545 presence or absence of thiazovivin. Percent confluence was measured 4 days after replate in

546 control, *PAWR* knockout and *PMAIP1* knockout cells. Bars represent mean from 3 independent

547 wells with 4 images per well. Error bars +/- 1 std. dev from 4 images per well from 3

548 independent wells. The dissociation induced survival of *PAWR* mutant hPSCs has been

549 replicated >3 times. (C) Time lapse microscopy of live cells during first 9 hours of replate.

550 Control and *PAWR* knockout hPSCs survive replating in the presence of thiazovivin by

551 extending cellular projections and forming an actin adhesion belt organized with stress fibers.

552 Phallodin stain at 3.5h in fixed cells. Control cells without thiazovivin have abundant membrane

553 blebbing and this is highlighted by the presence of small circular actin rings in phallodin stained

554 cells. *PAWR* mutants have reduced blebbing and an intermediate phallodin staining without

555 small actin rings. Scale bar = 50 uM (D) Immunofluorescence detects PAWR protein

556 colocalizing with F-ACTIN. Following dissociation PAWR protein colocalizes with F-ACTIN in the

557 presence of thiazovivin in adhesion belt like structures and in the absence of thiazovivin in

558 membrane blebs. In green PAWR protein. In magenta phallodin stained F-actin. In blue DAPI

559 stained nuclei. Scale bar = 50 uM

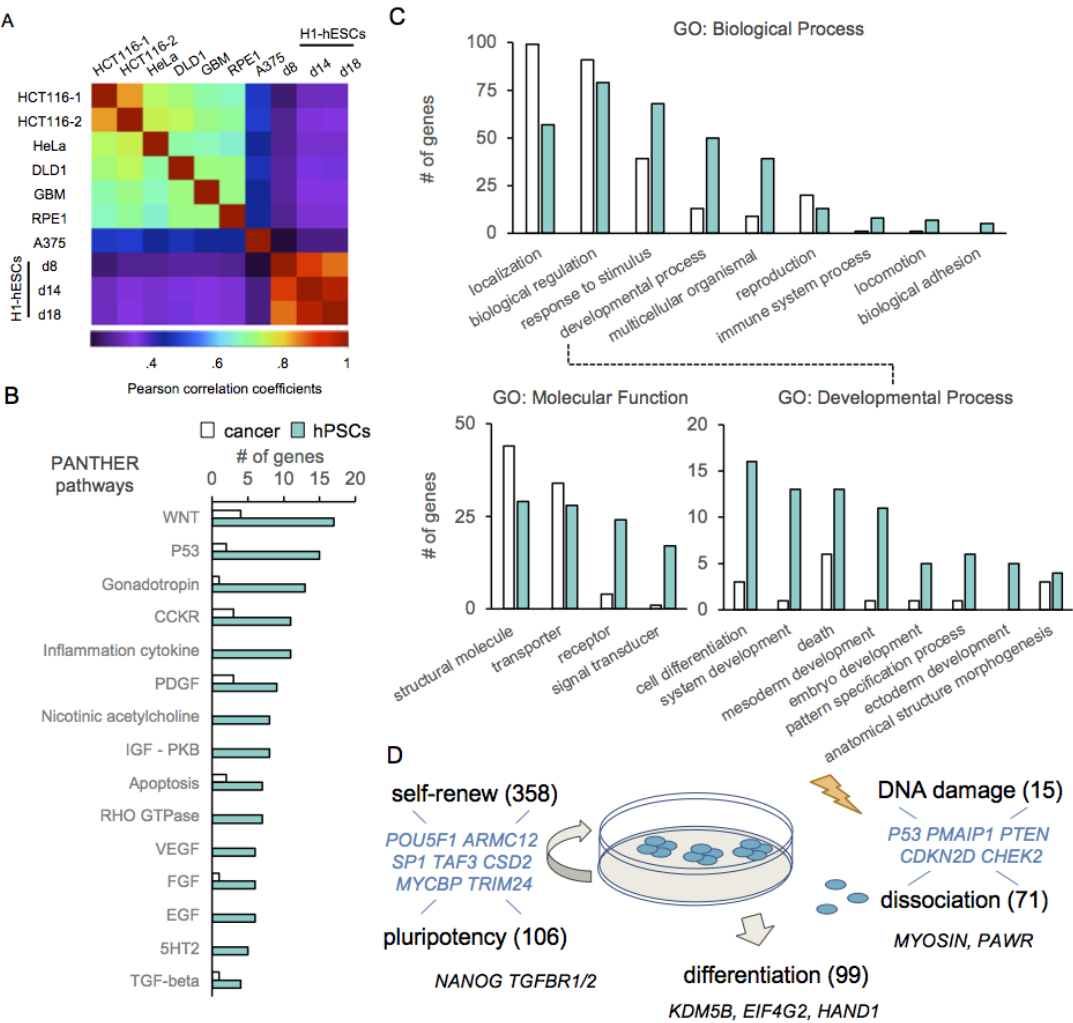560 **Figure 5: *PAWR* is required for dissociation-induced death**

561
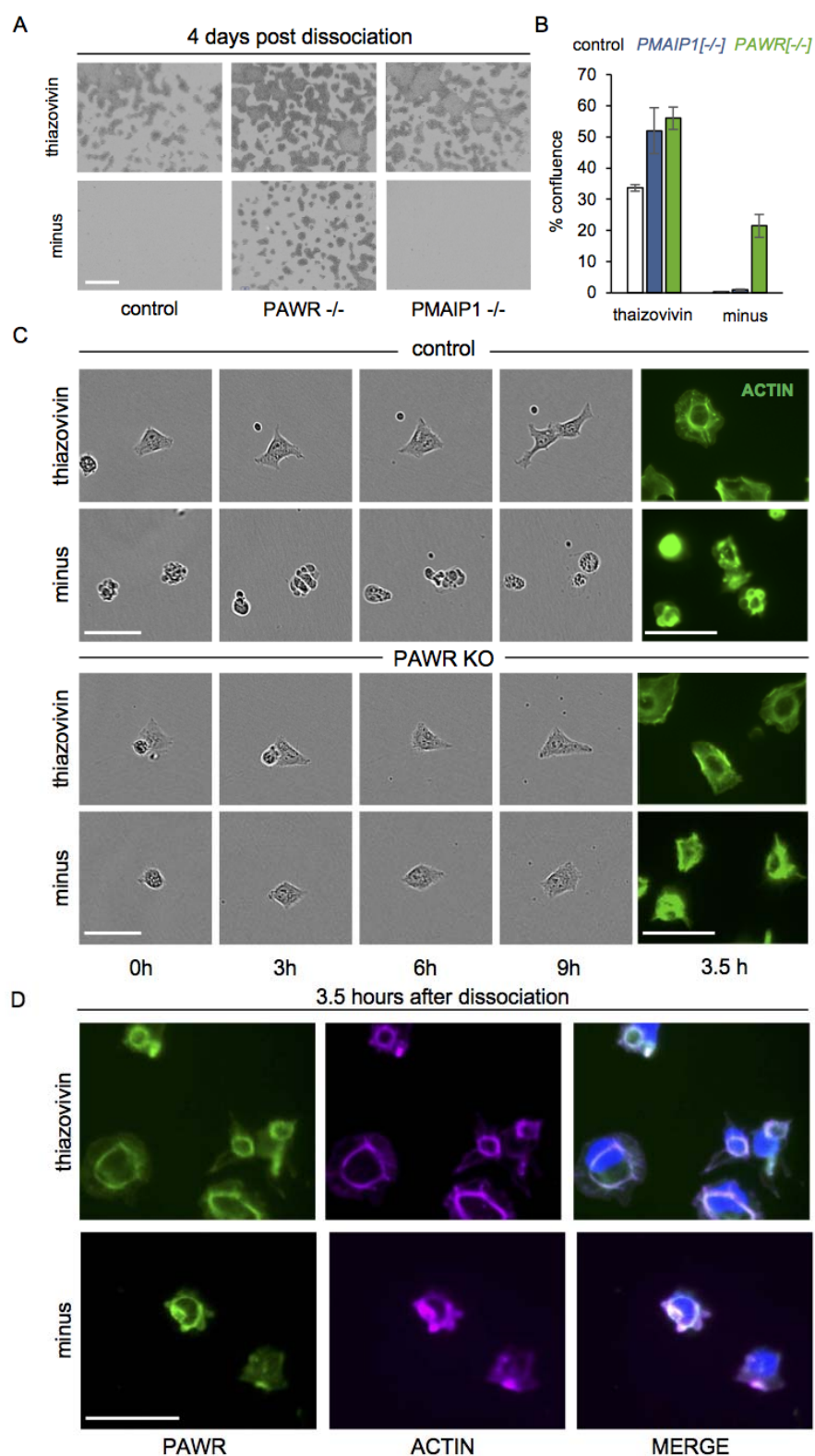
562 **Figure 6: OCT4 FACS-based screen identifies pluripotency gene network** (A) Diagram
563 depicting FACS-based CRISPR screen using an OCT4 specific antibody to sort OCT4 high- and
564 low-expressing cells. Cells were mutagenized with Cas9 for 8 days prior to FACS sorting, DNA
565 isolation and NGS was used to identify an enrichment of sgRNAs in the high and low OCT4
566 populations. (B) Scatter plot depict gene level results for genome-scale OCT4 FACS screen.
567 Green depict OCT4^{LOW} and gold depicts OCT4^{HIGH} enriched sgRNAs. Y-axis is a p-value
568 generated from RSA down/up analysis. X-axis marks the Z-score (Q1/Q3). (C) String-DB
569 analysis identifies a 20-gene network connected to *OCT4* among gene sgRNAs that were enrich
570 in cells with low OCT4 protein. Genes with published roles in pluripotency, reprogramming and
571 embryo development are highlighted in green.

572 **Figure 6: OCT4 FACS-based screen identifies pluripotency gene network**

573

574 **Figure 7: Identification of hPSC-specific essential gene networks** (A) Heatmap of Pearson

575 correlation coefficients adapted from Hart et al., 2015 to include CRISPR screening data in H1-

576 hESCs (B) PANTHER pathway analysis identified 92 enriched pathways in hPSCs. A subset of

577 15 hPSC-specific pathways are depicted. (C) Depiction of gene ontology categories including

578 biological processes, molecular functions and developmental processes that are specific to

579 hPSCs but not cancer cell lines. (D) Schematic of genes identified by CRISPR screening in

580 hPSCs and their putative functions. 770 fitness genes regulate the self-renewing potential of

581 hPSCs. 113 genes with low OCT4 protein are implicated in pluripotency, 99 genes with

582 increased OCT4 protein may promote differentiation. 20 genes are implicated in the toxic

583 response to DNA damage. 76 genes are implicated in the sensitivity of hPSCs to single-cell

584 dissociation. (B-D) Bioinformatic analysis of 829 core essentials cancer (white bars – Hart et.

585 al., 2015) and 653 hPSC-specific genes (green bars). Genes in multiple categories are shown in

586 blue.

587 **Figure 7: Identification of hPSC-specific essential gene networks**

588
589

595 **AUTHOR CONTRIBUTIONS**

596 R.J.I. and A.K designed all experiments and wrote the manuscript. M.R.S, K.A.W and R.D
597 revised manuscript. R.J.I. conducted live cell imaging, immunofluorescence, qPCR and Western
598 blotting S.K. and K.A.W. generated Ngn2-inducible cell lines and differentiated them into Ngn2
599 neurons. M.S. helped with genome-scale hPSC culture, packaged lentiviral sgRNAs and
600 generated CRISPRi lines. E. F. provided lentiviral supernatants and prepped DNA samples for
601 NGS. J. R. sequenced CRISPR indels. B.A. generated Precision/Recall values using the
602 BAGEL algorithm. S.K. generated RNA expression data in hPSCs and NGN2 neurons and it
603 was analyzed by R.R. G.R.H., Z.Y., and G.M. helped design pooled screen and performed
604 analysis. J. R-H. generated sgRNA libraries. C.R. sequenced pooled fitness screen samples.
605 S.P. sorted OCT4 high and low expressing cells by FACS. D.J.H. sequenced OCT4 FACS
606 screen.

607 **CONFLICTS OF INTEREST**

610

611   **SUPPORTING INFORMATION**

612

613   **Figure S1: Genome-scale screening in hPSCs** Paradigm for genome-scale pooled screen in

614   hPSCs. (A) hPSCs were transduced with 110,000 lentiCRISPRs in 5-layer CellSTACKs.

615   Following expansion and hPSC CRISPR library banking cells were subjected to subsequent

616   screens depicted in B-D. (B) Fitness screen in hPSCs. Cells were exposed to Cas9 (+dox) for a

617   total of 12 days to ensure complete gene disruption. DNA samples were taken at 0, 8, 14 and

618   18 days after exposure to Cas9. (C) Positive selection screen for suppressor of dissociation-

619   induced cell death. At the end of the fitness screen the genome-scale hPSCs mutant CRISPR

620   library was replated in the absence of ROCK inhibitors (- thiazovivin). After two weeks cells that

621   suppressed dissociation-induced death were collected for DNA isolation. (D) FACS-Based

622   CRISPR screen for regulators of OCT4 protein expression. hPSC CRISPR cell library was

623   thawed and exposed to Cas9 (+ dox) for 8 days before cell sorting to select for cells with high or

624   low expression of OCT4 protein.

Figure S1: Genome-scale screening in hPSCs
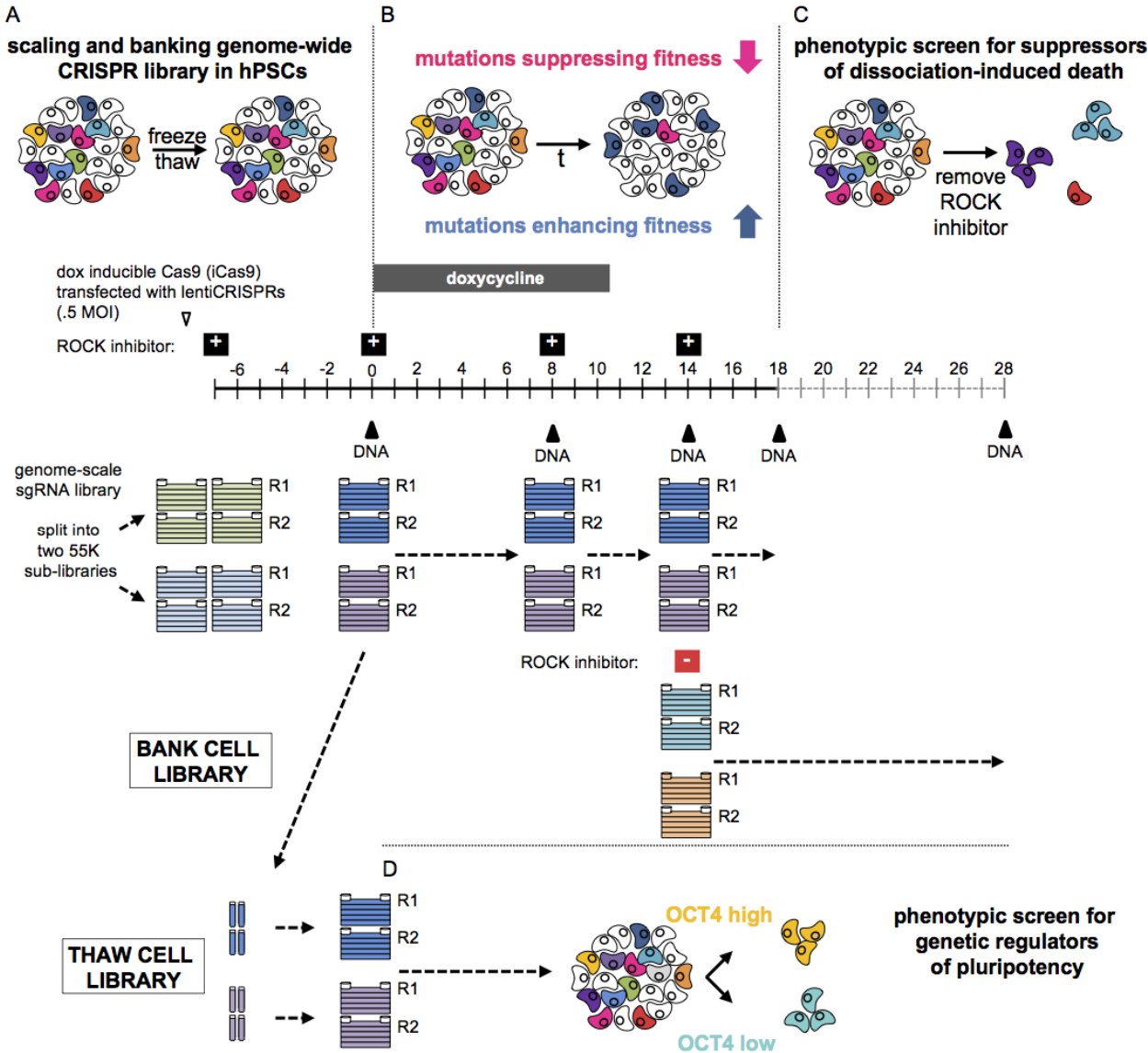
628   **Figure S2: Enrichment of sgRNAs on X and Y chromosomes** (A) Bar chart shows the

629   chromosomal distribution of the top 770 depleted (Files S3) and 946 enriched (RSA-up < -2.25,

630   File S6. (B) NGS quantification indels induced by sgRNAs targeting the X chromosome. Control

631   reads are represented by white bars, in-frame mutations by light blue bars and frameshift

632   mutations by dark blue bars. n=1 DNA sample per sgRNA and cell line. >20,000 sequencing

633   reads per sample.

634 **Figure S2: Enrichment of sgRNAs on X and Y chromosomes**

635
636
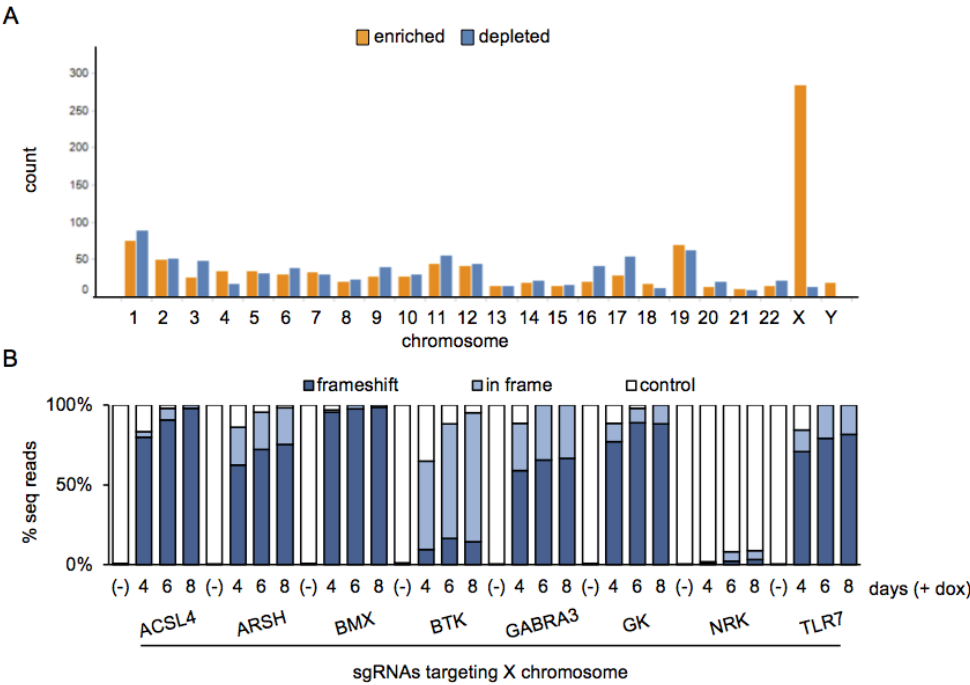
637   **Figure S3: *PMAIP1* knock out hPSCs** (A) iCas9 H1-hESCs were treated with Cas9 RNPs

638   targeting *PMAIP1*. NGS analysis demonstrated that complete knockout of *PMAIP1* was

639   achieved with a spectrum of frameshift indels disrupting *PMAIP1*. n=1 sample, 2627 sequencing

640   reads (B) *PMAIP1* mutations suppress DSB induced toxicity. Whole well images from 24-well

641   plates during editing with *MAPT* sgRNA in H1-iCas9 control and PMAIP1 mutant backgrounds.

642   Confluency mask in green. (C) DNA isolated after 10 of doxycycline treatment shows that on-

643   target *MAPT* editing efficiency is similar between control and *PMAIP1* mutant pools. Control

644   reads are represented by white bars, in-frame mutations by light blue bars and frameshift

645   mutations by dark blue bars. n=1 day 0 samples, n= 2 day 10 samples, >20,000 sequencing

646   reads per sample.

647 **Figure S3: *PMAIP1* knock out hPSCs**

648
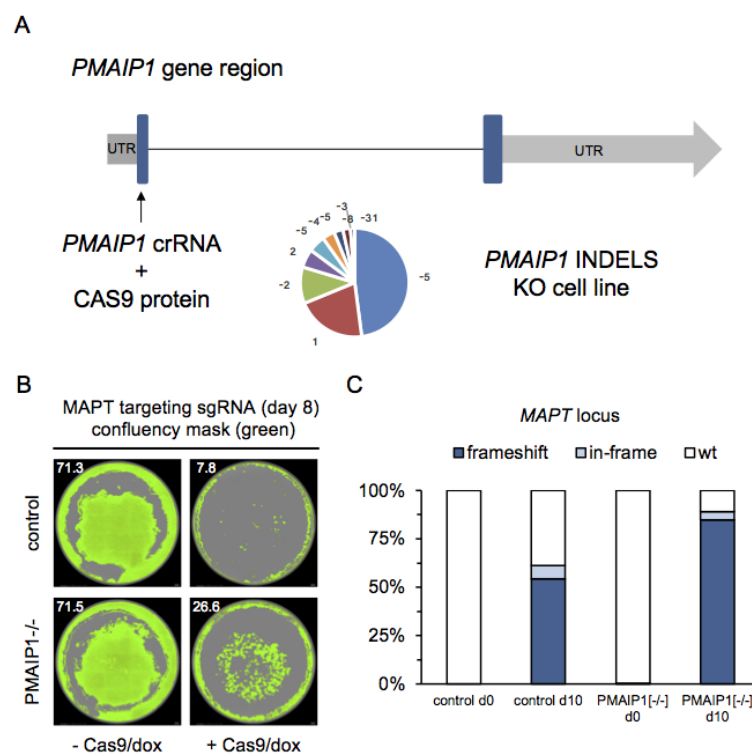
649 **Figure S4: *PAWR* is required for dissociation-induced death** (A) iCas9 expressing H1-
650 hESCs were infected with lentiCRISPRs targeting *PAWR*. PAWR mutant pools were created by
651 exposing cells to Cas9/dox for one week. After mutagenesis, control and mutant cells were
652 dissociated using accutase and replated plus or minus thiazovivin. Control cells die without
653 thiazovivin while PAWR mutants survive. Images were taken 4 days after dissociation. (B) H1-
654 hESC constitutively expressing dCas9-KRAB were infected with CRISPRi sgRNAs targeting the
655 promoter of *PAWR*. 3 out of 4 sgRNAs (i1, i2, i3, i5) tested were able to survive a replate in the
656 absence of thiazovivin while controls died. Images were taken 6 days after dissociation. (C)
657 iCas9 H1-hESCs were treated with Cas9 RNPs targeting *PAWR*. NGS analysis demonstrated
658 that complete knockout of *PAWR* was achieved with a spectrum of frameshift indels disrupting
659 *PAWR*. n=1 samples, 2621 sequencing reads (D) Karyotype analysis revealed that *PAWR*
660 mutants retain a normal Karyotype. (E) *PAWR* mutants do not suppress DNA damage-induced
661 cell death. Live imaging of confluence in *MAPT* sgRNA expressing iCas9 cells +/- DSB
662 (+dox/Cas9) in control, *PMAIP1$^{-/-}$* knockout cells, and *PAWR$^{-/-}$* knockout cells. *PAWR$^{-/-}$*, *P21$^{-/-}$*
663 knockout and control hPSCs die upon DSB induction while *PMAIP1$^{-/-}$* mutants survive. Black
664 lines indicate control, blue lines indicate *PMAIP1$^{-/-}$* mutants, green lines indicate *PAWR$^{-/-}$*
665 mutants, orange lines indicate *P21$^{-/-}$* mutants. Solid lines are without dox and dashed lines are
666 cultured with Cas9 (+dox). Y-axis is percent confluency each point represents mean of 3
667 independent whole-well images. error bars +/- 1 std. X-axis time in days of treatment. (A) *PAWR*
668 is highly expressed in hESCs and iPSCs. Y-axis represents expression in Transcripts Per
669 Kilobase Million (TPM). H1-hESCs (n=1), H9-hESCs (n=3), 8402-iPSCs (n=3) and HDFn-iPSCs
670 (n=4). X-axis represents days after induction of a doxycycline inducible NGN2 expression
671 cassette.

672 **Figure S4:** *PAWR* **is required for dissociation-induced death**
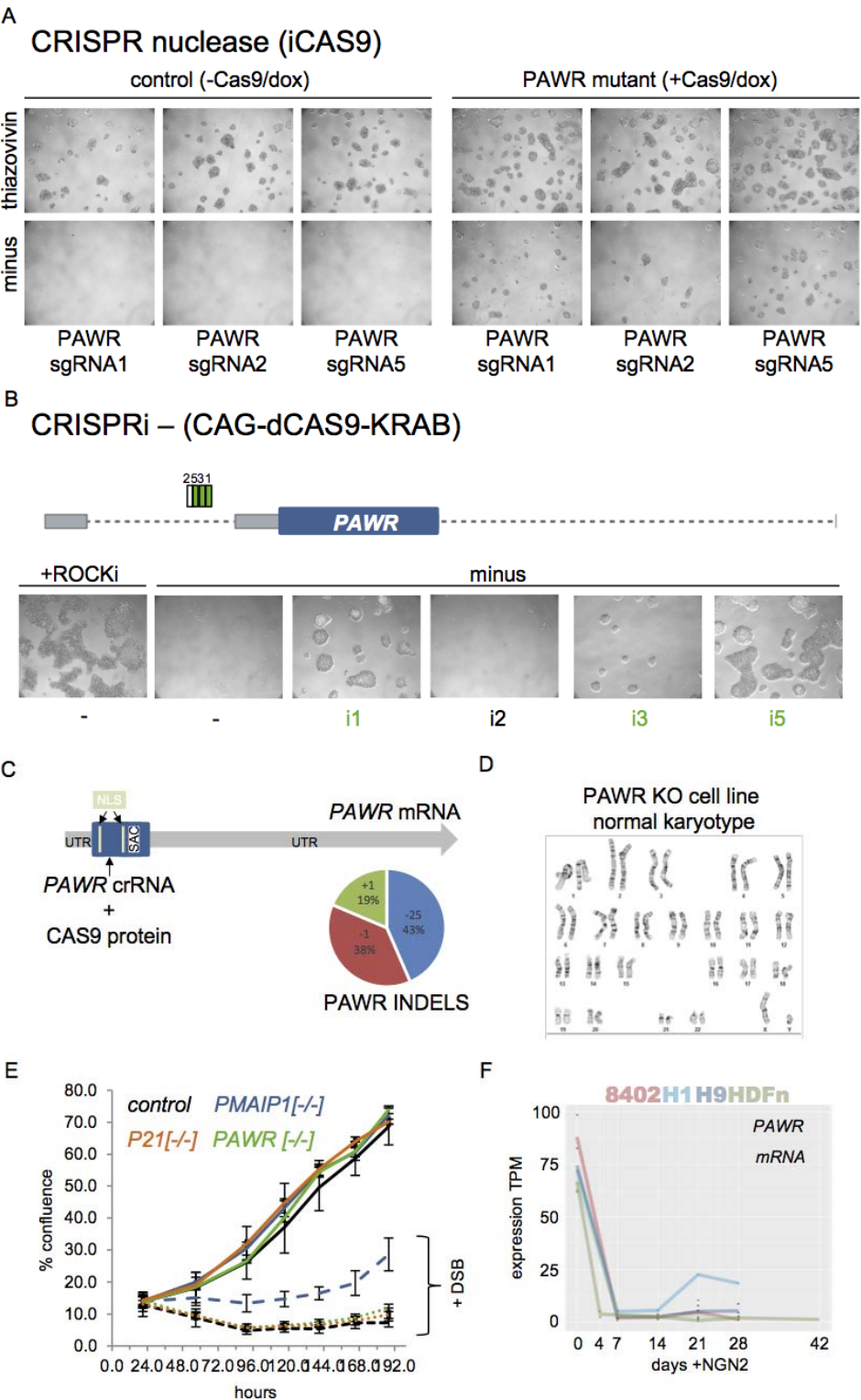
675 **Figure S5: PAWR is induced after dissociation and required for caspase activation** (A)

676 Immunofluorescence using PAWR antibodies detects protein after dissociation but not in

677 confluent colonies. PAWR protein in green. DAPI stained nuclei in blue. Scale bar = 100 uM (B)

678 Immunofluorescence using PAWR antibodies detects protein after dissociation in controls but

679 not *PAWR* knockout cells. (C) In control cells western blot detects caspase activation 4 hours

680 after dissociation in the absence of thiazovivin. *PAWR* mutants do not exhibit caspase

681 activation. In green anti-rabbit Cleaved Caspase-3 (CC3, 17 and 19 kDa) antibodies. In red anti-

682 mouse GAPDH (37 kDa) loading control.

683

684 **Figure S5: PAWR is induced after dissociation and required for caspase activation**

685

40
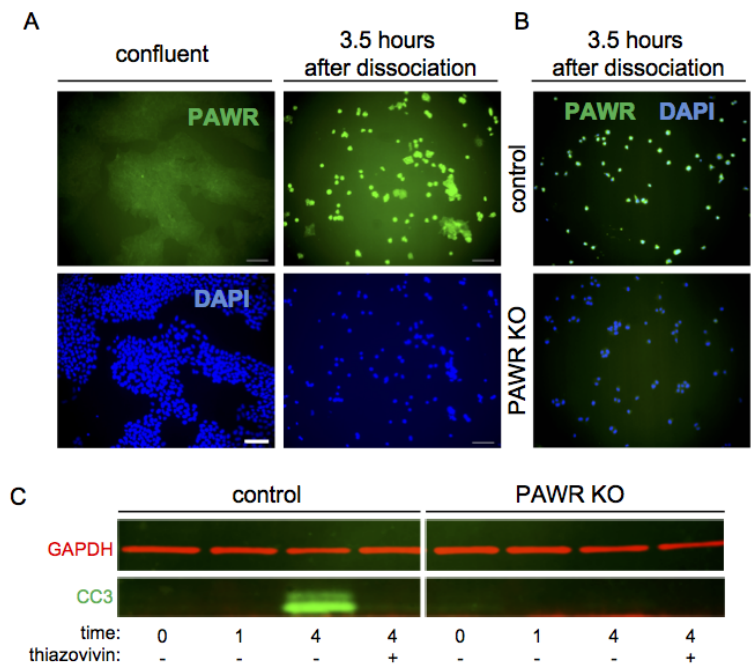
686 **Figure S6: PRKCZ and SCRIB proteins are expressed in dissociated hPSCs** (A)

687 Immunofluorescence detects PRKCZ and SCRIB proteins localizing to membrane blebs in the

688 absence of thiazovivin. In the presence of thiazovivin PRKCZ and SCRIB demonstrate a nuclear

689 or perinuclear localization respectively. In green PRKCZ and SCRIB proteins. In blue DAPI

690 stained nuclei. White scale bar = 20 uM.

691 **Figure S6: PRKCZ and SCRIB proteins are expressed in dissociated hPSCs**

692
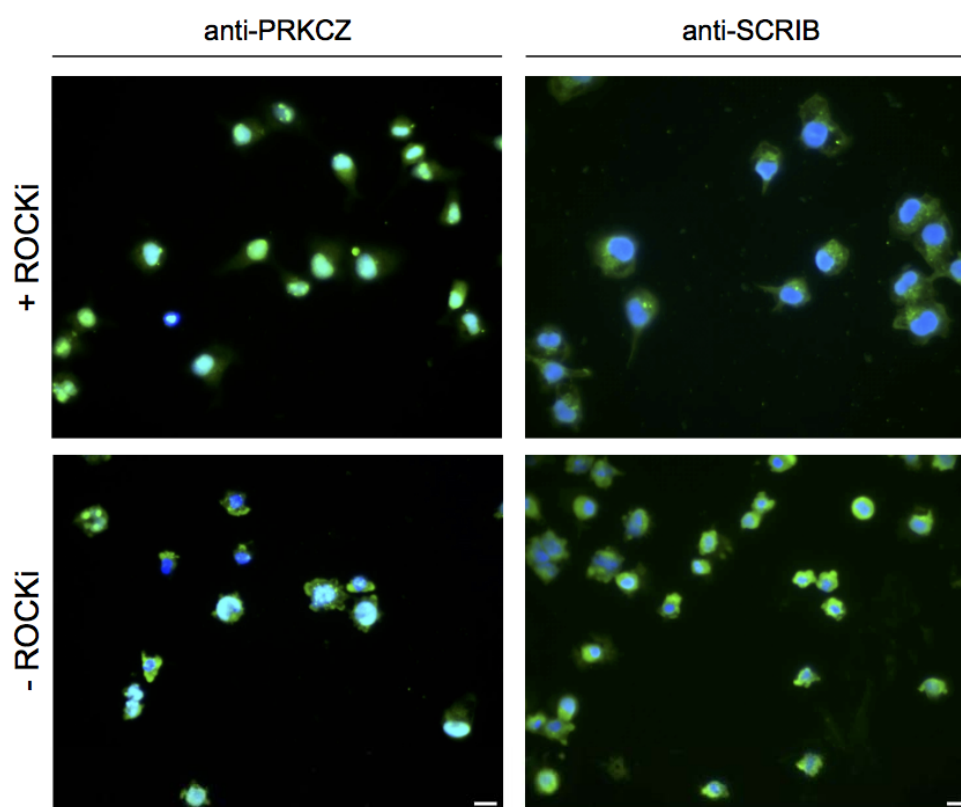
693 **MATERIALS AND METHODS**

694 **Cell lines**

695 H1-hESCs (WA01-NIHhESC-10-0043) and H9-hESCs (NIHhESC-10-0062) were obtained from

696 WiCell. 8402-iPSCs originated from GW08402 fibroblasts from the Coriell Institute and

697 reprogrammed as described by Sun et al., 2016(Sun et al., 2016). hDFN-iPSCs were generated

698 as described by Bidinosti et. al., 2016 (Bidinosti et al., 2016). hPSC lines were free of

699 Myoplasma and tested using the Mycoalert Detection kit (Lonza). SNP fingerprinting confirmed

700 the identify of hPSC lines used. Karyotyping was performed by Cell Line Genetics (Madison,

701 WI).

702 **Genome Engineering**

703 H1-hESCs expressing dox inducible (i) iCas9 were generated by Ihry et. al., 2018. Dox treated

704 H1-iCas9 cells were subjected to three successive rounds of RNAimax delivery of the two-

705 component synthetic crRNA/tracrRNA (IDT) pairs targeting *PMAIP1*, *PAWR* and *TP53* as

706 described by Ihry et al., 2018. *PMAIP1*, and *PAWR* were transfected with a single sgRNA while

707 *TP53* was co-transfected with 3 crRNAs. CRISPR indel analysis detected effcient gene

708 disruption for all three genes and was performed as described by Ihry et. al., 2018.

709 PMAIP1 crRNA 3   TCGAGTGTGCTACTCAACTC

710 PAWR crRNA 5   CGAGCTCAACAACAACCTCC

711 TP53 crRNA 1   GAAGGGACAGAAGATGACAG

712 TP53 crRNA 2   GAAGGGACAGAAGATGACAG

713 TP53 crRNA 4   GAGCGCTGCTCAGATAGCGA

714 P21 crRNA 1   AATGGCGGGCTGCATCCAGG

715 P21 crRNA 4   TCCACTGGGCCGAAGAGGCGG

716 P21 crRNA 6   GGCGCCATGTCAGAACCGGC

717 **Pooled Mutagenesis (CRISPR nuclease/interference)**

718 H1-hESCs expressing a constitutive (c) Cas9-KRAB knocked-in to the AAVS1 locus were

719 generated as described by Ihry et., al., 2018. The following lentiCRISPR were used to transduce

720 iCas9 or cCas9-KRAB cells to generate mutant cell pools.

721 CRISPR nuclease

722 PAWR sgRNA 1   TTTGGGAATATGGCGACCGG

723 PAWR sgRNA 2   GGTGGCTACCGGACCAGCAG

724 PAWR sgRNA 5   CGAGCTCAACAACAACCTCC

725 MAPT sgRNA 1   GAAGTGATGGAAGATCACGC

726 ACSL4 sgRNA   TGGTAGTGGACTCACTGCAC

43

727	ARSH sgRNA	GCAGCACCGTGGCTACCGCA
728	BMX sgRNA	ATGAAGAGAGCCGAAGTCAG
729	BTK sgRNA	GGAATCTGTCTTTCTGGAGG
730	GABRA3 sgRNA	AAGGACTGACCTCCAAGCCC
731	GK sgRNA	TAGAAAGCTGGGGCCTTGGA
732	NRK sgRNA	CGCCTTCCTATTTCAGGTAA
733	TLR7 sgRNA	CAGTCTGTGAAAGGACGCTG
734	CRISPR interference	
735	PAWR sgRNA 1	GGCGCGCTCGAGGACTCCAA
736	PAWR sgRNA 2	GTTGCAGGGTGGGGACCCGG
737	PAWR sgRNA 3	GCTGGCCGGTAGTGACTGGT
738	PAWR sgRNA 5	GGCTGCTGGCCGGTAGTGAC

739 **Large-scale culture of hPSC**

740 H1-hESCs with AAVS1 knock in of the iCas9 transgene were generated and cultured in TeSR-

741 E8 media (STEMCELL TECH.-05940) on vitronectin (Gibco-A14700) coated plates as

742 described by Ihry et. al., 2018. Pilot studies with a sub-genome sgRNA library used a total of 40

743 individual T225 flasks and was cumbersome (Ihry et. al., 2017). Daily feeding and passaging in

744 which multiple flask needed to be pooled was time consuming and increased the risk for

745 contamination. To minimize the manipulation required during feeding and passaging we used 5-

746 layer CellSTACKs. The vessels are large enough to contain an entire 55,000 sgRNA at roughly

747 1000x coverage per sgRNA at a seeding density of 21,000 cells/cm^{2} (Seed 66 million cells for

748 ~1200x). In practical terms only 4 to 8 5-layer CellSTACKs were growing at a given time during

749 the month-long genome-scale CRISPR screen (Fig. S1). Given the expense of E8 media

750 Penicillin-Streptomycin (pen/strep) at 100 U/mL was added as an additional insurance policy for

751 the first screen at scale. After running a lengthy genome-scale screen and becoming

752 experienced with large-scale hPSC culture it is possible to run future screens without pen/strep

753 (Fig. S2).

754 **lentiCRISPR packaging**

755 For a one-layer CellSTACK 42 million HEK293T (66,000 cells/cm^2) were plated in 100 mL of

756 media (DMEM +10% FBS + 1x NEAA, no pen/strep). One day after seeding, cells were

757 transfected with single lentiCRISPR plasmids in 6-well plates or pooled lentiCRISPR plasmids in

758 CellSTACKs. For a one-layer CellSTACK 102 uL of room temp TransIT (Mirus MIR 2700) and

759 3680 uL Opti-MEM (Invitrogen 11058021) were mixed incubated in a glass bottle for 5 minutes

760 at room temp. 94.5 ug of Lentiviral Packaging Plasmid Mix (Cellecta CPCP-K2A) and 75.6 ug of

761   the lentiCRISPR plasmid library was added to the transfection mix and incubated for 15 minutes

762   at room temp. After incubation, the mix was added to 100 mL of fresh media and the cells were

763   fed. The next day the transfected cells received 100 ml fresh media. After 3 days of viral

764   production supernatants were filtered (.45uM corning 430516) and aliquoted in to 1ml tubes for

765   storage at -80 C.

766   **Large-scale transduction of hPSC**

767   We conducted a genome-scale CRISPR screen using a 110K sgRNA library (~5 sgRNAs per

768   gene, split into two 55K sgRNA sub-pools, DeJesus et al., 2016). We desired 1000x coverage of

769   each sgRNA to offset cell loss from double strand break (DSB)-induced toxicity (Ihry et. al.,

770   2017). To screen a sufficient number of cells we infected hPSCs with lentiCRISPRs in 5-layer

771   CellSTACKs. Cells were infected at .5 MOI to ensure each cell was infected with no more than a

772   single sgRNA. After puromycin selection cells were expanded for one week without dox to be

773   pelleted for DNA, banked or screened (Fig. 1A, S1).

774   Pooled CRISPR screens rely on cells being efficiently transduced at less than or equal

775   to .5 MOI. We developed a reverse transfection method for hPSCs without polybrene that

776   resulted in an efficient transduction with low volume exposure to HEK293T lentiviral

777   supernatants. LentiCRISPR plasmids expressed a constitutive RFP and puromycin resistance

778   to mark and select for infected cells respectively. Viral titer of the two 55,000 sgRNA libraries

779   expressing RFP in 6-well plates determined that less than 25 uL in 1.5mL of media was required

780   for .5 MOI. These calculations scaled appropriately in 5-layer cell stacks with 500 mL of media

781   and approximately 50% of the cells were RFP positive in the absence of puromycin.

782   A genome-scale lentiCRISPR library targeting each gene 5 times has been split into

783   55,000 sub-pools (pool 1 and 2). To screen at 1000x per sgRNA, 264 million hPSCs are

784   infected in 4x 5-layer CellSTACKS (12,720 cm^2, 21,000 cells/ cm^2). Cells are infected at .5 MOI

785   to ensure only one sgRNA is expressed per cell (+sgRNA/puro^R/RFP). After puromycin

786   selection cells are expanded until confluent (4-6 days). At this point 40 million cells (10

787   million/ml) can be banked in 5ml cryovials for use at a later date.

788   **Banking lentiCRISPR infected hPSC library**

789   One 5-layer cell stack was treated with 200 mL accutase that was evenly distributed

790   among layers. After incubation at 37 C for 10 minutes, accutase (Gibco-A1110501) was

791   neutralized with 200 mL E8 media. Cells were counted and pelleted to be resuspended at a

792   concentration of 10 million cells per ml in a solution of 40% Tet-free FBS (Seradigm #1500-500)

793   and 10% DMSO (Sigma D2650) and 50% E8 media. 4 ml aliquots were placed in 5 ml cryovials

794   and frozen in a Mr. Frosty (Thermo Scientific 5100-0050) at -80 C overnight before long-term

795   storage in liquid nitrogen. Thawing of cells banked in 5ml cryovials showed an average viability

796   around 85% for both lentiCRISPR pools. Viability was assayed using a Nexcelom Cellometer

797   Auto 2000 and AO/PI (Nexcelom CS2-0106) staining solution.

798   We tested the effect of freezing and thawing on the representation of the sgRNAs in the

799   library by thawing the cell library at either 700x (40 million cells per 55k sub-pool) or 2100x (120

800   million cells per 55k sub-pool) cells per sgRNA. Cells were thawed in a 37 C water bath and

801   transferred to a 50mL conical with E8 media and centrifuged at 300 g for 3 minutes. Pelleted

802   cells were resuspended in E8 media and replated at a density of 30 to $40*10^6$ cells/cm^2. 3

803   cryovials with 120 million cells was thawed and plated on a 5-layer cell stack (120,000,000

804   /55,000 = 2100x).

805   After thawing and feeding the cells for two days, DNA was isolated and analyzed by

806   NGS to measure the representation of each sgRNA in the pool. Each sample was compared to

807   the original lentiCRISPR plasmid library to generate a log_2(fold change) value. Both day zero

808   and freeze/thaw samples had an over 87% alignment of sequencing reads and fewer than 25

809   missing barcodes per replicate. Calculating the log2(fold change) revealed no significant change

810   in the representation of sgRNAs before (day 0) or after one freeze/thaw cycle. Pearson

811   correlation analysis demonstrated there was a high correlation between the day zero samples

812   and the freeze/thaw samples (Fig. 1B).

813   **OCT4 FACS-BASED screen**

814   Cells were dissociated using accutase for 10 min at 37 C to create a single-cell suspension

815   which was strained using a 40-micron filter and was counted. After removing accutase, pelleted

816   cells were resuspended in a volume of 1 million cells/mL for the staining protocol. For each

817   replicate 55 million unsorted cells were frozen down prior to fixation. The remaining cells were

818   fixed in 4% PFA in PBS for 10 minutes at room temperature on a rocker. Cells were spun down

819   at 300 RCF for 3 min between each subsequent solution change. Cells were washed with .1%

820   Triton-X in PBS after fixation and blocked in 2% goat serum, .01% BSA and .1% triton X in PBS

821   for 1hr at room temperature. Conjugated (AF488) primary antibodies specific to OCT4 (CST

822   5177) were diluted in blocking solution (1:200) and incubated with cells on a rocker over night at

823   4 C. Prior to FACS analysis cells were resuspended in PBS at a concentration of 30 million

824   cells/mL. A total of 1.2 billion cells were sorted into OCT4^{low} (50 million cells) and OCT4^{high} (61

825   million cells) populations using an ARIA III (BD).

826   **DNA isolation**

827   For each replicate, 55 million cells (1000x) were pelleted and genomic DNA was isolated using

828   QIAamp DNA Blood Maxi Kit (Qiagen 51194) as directed by manufacturer. Isolating genomic

829   DNA from 4% PFA fixed cells was performed by utilizing phenol chloroform extraction. Cells

830   were resuspended in 500ul TNES (10mM Tris-Cl ph 8.0, 100mM NaCL, 1mM EDTA, 1% SDS)

831   and incubated overnight at 65 C. After allowing the samples to cool, 10ul of RNase A (Qiagen

832   19101) and samples were incubated at 37 C for 30 minutes. Next, 10ul of proteinase K (Qiagen

833   19133) and incubated for 1 hour at 45 C. Add 500ul of PCIA (Phenol;Cholorform;Isoamyl

834   alcohol ph 8) (Thermo 17908) and vortex. Spin samples in a centrifuge at max speed for 2

835   minutes. Transfer the aqueous phase to 500ul of PCIA and vortex. Spin at max speed for 2

836   minutes. Transfer the aqueous phase to 450ul of chloroform and vortex. Spin at max speed for

837   2 minutes. Transfer aqueous phase to 40ul of 3M NaAcO ph 5.2. Add 1 ml of 100% ethanol, mix

838   and precipitate DNA for 1 hour on ice. Spin at max speed for 2 minutes. Decant and wash with

839   1ml 70% ethanol. Spin at max speed for 1 minutes. Decant and air dry the pellet. Resuspend in

840   50ul of nuclease free H_2O.

841   **mRNA expression**

842   qPCR and RNA-seq analysis were performed as described by Ihry et. al., 2018. Median TPM

843   values for H1-hESCs are available upon request. RNA-seq data for in 4 iPSC control lines

844   subjected to NGN2 differentiation is available upon request but is restricted to the expression for

845   *PAWR* and *PMAIP1*.

846   **Assaying sensitivity to DNA damage**

847   Control and mutant iCas9 H1-hESCs expressing a *MAPT* targeting sgRNA were monitored daily

848   post-media change using an IncuCyte zoom (Essen Biosciences). At the onset of the

849   experiment cells were plated at density of 10,500 to 21,000 cells/cm^2 and cultured plus or minus

850   dox for the duration. Confluence was calculated using the processing analysis tool (IncuCyte

851   Zoom Software).

852   **Assaying survival without ROCK inhibitor**

853   Control and mutant iCas9 H1-hESCs were dissociated with accutase for 10 minutes. Flowmi 40-

854   micron cell strainers (BEL-ART H13680-0040) were used to ensure a uniform single-cell

855   suspension prior to replating cells. Cells were plated at a density of 10,500 to 21,000 cells/cm^2

856   plus or minus thiazovivin (ROCK inhibitor). Timelapse images were taken in 3 hr intervals using

857   IncuCyte zoom (Essen Biosciences). The confluence processing analysis tool (IncuCyte Zoom

858   Software) calculated confluency for each sample.

859   **Immunofluorescence and Western Blotting**

860   Immunofluorescence staining of fixed cells was performed as described by Ihry et. al., 2018.

861   Protein lysates were made by vortexing cell pellets in RIPA buffer (Thermo Scientific 89901)

862   supplemented with Halt protease inhibitor cocktail (Thermo Scientific 78430) and phosphatase

863   inhibitors (Thermo Scientific 1862495). Samples were incubated at 4C for 10 minutes before

864   centrifugation at 14,000 x g for 10 minutes at 4C. Supernatants were transferred to new tubes

865   and quantified using the BCA protein assay kit (Thermo Scientific 23225) and a SpectraMax

866   Paradigm (Molecular Devices) plate reader. Samples were prepared with NuPAGE LDS sample

867   buffer 4x (Invitrogen NP0008) and NuPAGE sample reducing agent (Invitrogen NP0009) and

868   heated for 10 minutes at 70 C. Chameleon Duo Pre-stained Protein Ladder (LiCOR P/N 928-

869   60000) was loaded alongside 10 ug of protein per sample on a NuPAGE 4-12% Bis-Tris Protein

870   Gels, 1.5 mm, 10-well (Invitrogen NP0335BOX). Gel electrophoresis was performed at 150 V for

871   1hr in NuPAGE MOPS SDS Running buffer (20X) (Invitrogen NP0001) using a XCell SureLock

872   Mini-Cell (Thermo Scientific EI0002). Transfer was performed using an iBlot 2 dry blotting

873   system (Thermo IB21002 and IB23002) as described by manufacturer. Blots were blocked in

874   TBS blocking buffer (LiCOR 927-50000) for 1 hour at room temperature. The blots were then

875   incubated with primary antibodies diluted in TBS over night at 4 C. Blots were washed 3X in

876   PBST and incubated with secondary antibodies diluted in TBS for 2 hours at room temperature.

877   Blots were imaged using an Odyssey CLx (LiCOR).

878   <u>Primary antibodies</u>

879   Phallodin-647 (ThermoFisher Scientific A22287) - 1:40

880   SCRIB (Abcam ab36708) - 1:100 (IF)

881   PRKCZ (Abcam ab59364) - 1:100 (IF)

882   PAWR/PAR-4 (CST-2328) - 1:100 (IF)

883   Cleaved Caspase-3 Asp175 (CST-9661) - 1:200 (IF) 1:1000 (WB)

884   GAPDH (Enzo ADI-CSA-335-E) - 1:1000 (WB)

885   aTUB (Sigma 76199) - 1:10000 (WB)

886   <u>Secondary Antibodies</u>

887   IRDye 800CW anti-rabbit (LiCOR 926-32211) - 1:5000

888   IRDye 680RD anti-mouse (LiCOR 926-68070) - 1:5000

889   AF488 conjugate Goat anti-Rabbit IgG (H+L) (ThermoFisher-A-11008) - 1:500

890   **DATA AVAILABILITY**

891   Raw data and results generated for human pluripotent stem cells is available upon request. File

892   S1 includes log2 fold changes values for each sgRNA across conditions. File S2 and S6

893   includes RSA-up and -down values for the fitness screen and File S8 has RSA values for the

894   OCT4 FACS screen.

895   **CODE AVAILABILITY**

896 RNA-seq data processing and pooled CRISPR NGS was conducted using open source

897 software.

898

899 **REFERENCES**

900 1. Aguirre, A.J., Meyers, R.M., Weir, B.A., Vazquez, F., Zhang, C.-Z., Ben-David, U., Cook,

901   A., Ha, G., Harrington, W.F., Doshi, M.B., et al. (2016). Genomic copy number dictates a

902   gene-independent cell response to CRISPR-Cas9 targeting. Cancer Discov. *2641*, 617–

903   632.

904 2. Amir, H., and Laurent, L.C. (2016). Spontaneous Single-Copy Loss of TP53 in Human

905   Embryonic Stem Cells Markedly Increases Cell Proliferation and Survival HADAR.

906   2098–2110.

907 3. Amps, K., Andrews, P.W., Anyfantis, G., Armstrong, L., Avery, S., Baharvand, H., Baker,

908   J., Baker, D., Munoz, M.B., Beil, S., et al. (2011). Screening ethnically diverse human

909   embryonic stem cells identifies a chromosome 20 minimal amplicon conferring growth

910   advantage. Nat. Biotechnol. *29*, 1132–1144.

911 4. Bidinosti, M., Botta, P., Kröttner, S., Proenca, C.C., Stoehr, N., Bernhard, M., Fruh, I.,

912   Mueller, M., Bonenfant, D., Voshol, H., et al. (2016). CLK2 inhibition ameliorates autistic

913   features associated with SHANK3 deficiency. Science (80-.). *351*, 1199–1203.

914 5. Brill, L.M., Xiong, W., Lee, K.-B., Ficarro, S.B., Crain, A., Xu, Y., Terskikh, A., Snyder,

915   E.Y., and Ding, S. (2009). Phosphoproteomic Analysis of Human Embryonic Stem Cells.

916   Cell Stem Cell *5*, 204–213.

917 6. Burikhanov, R., Zhao, Y., Goswami, A., Qiu, S., Schwarze, S.R., and Rangnekar, V.M.

918   (2009). The Tumor Suppressor Par-4 Activates an Extrinsic Pathway for Apoptosis. Cell

919   *138*, 377–388.

920 7. Chambers, I., Silva, J., Colby, D., Nichols, J., Nijmeijer, B., Robertson, M., Vrana, J.,

921   Jones, K., Grotewold, L., and Smith, A. (2007). Nanog safeguards pluripotency and

922   mediates germline development. Nature *450*, 1230–1234.

923 8. Chen, G., Hou, Z., Gulbranson, D.R., and Thomson, J.A. (2010). Actin-myosin

924   contractility is responsible for the reduced viability of dissociated human embryonic stem

925   cells. Cell Stem Cell *7*, 240–248.

926 9. Chen, G., Gulbranson, D.R., Hou, Z., Bolin, J.M., Ruotti, V., Probasco, M.D., Smuga-

927   Otto, K., Howden, S.E., Diol, N.R., Propson, N.E., et al. (2011). Chemically defined

928   conditions for human iPSC derivation and culture. Nat. Methods *8*, 424–429.

929 10. Chia, N., Chan, Y., Feng, B., Lu, X., Orlov, Y.L., Moreau, D., Kumar, P., Yang, L., Jiang,

930   J., Lau, M., et al. (2010). A genome-wide RNAi screen reveals determinants of human
931   embryonic stem cell identity. Nature *468*, 316–320.

932 11. Cong, L., Ran, F.A., Cox, D., Lin, S., Barretto, R., Habib, N., Hsu, P.D., Wu, X., Jiang,
933   W., Marraffini, L.A., et al. (2013). Multiplex genome engineering using CRISPR/Cas
934   systems. Science *339*, 819–823.

935 12. DasGupta, R., Kaykas, A., Moon, R., and Perrimon, N. (2005). Functional genomic
936   analysis of the Wnt-wingless signaling pathway. Science (80-.). *308*, 826–833.

937 13. Díaz-Meco, M.T., Municio, M.M., Frutos, S., Sanchez, P., Lozano, J., Sanz, L., and
938   Moscat, J. (1996). The product of par-4, a gene induced during apoptosis, interacts
939   selectively with the atypical isoforms of protein kinase C. Cell *86*, 777–786.

940 14. Echeverri, C.J., Beachy, P.A., Baum, B., Boutros, M., Buchholz, F., Chanda, S.K.,
941   Downward, J., Ellenberg, J., Fraser, A.G., Hacohen, N., et al. (2006). Minimizing the risk
942   of reporting false positives in large-scale RNAi screens. Nat. Methods *3*, 777–779.

943 15. Gutekunst, M., Mueller, T., Weilbacher, A., Dengler, M.A., Bedke, J., Kruck, S., Oren,
944   M., Aulitzky, W.E., and Van Der Kuip, H. (2013). Cisplatin hypersensitivity of testicular
945   germ cell tumors is determined by high constitutive noxa levels mediated by oct-4.
946   Cancer Res. *73*, 1460–1469.

947 16. Haapaniemi, E., Botla, S., Persson, J., Schmierer, B., and Taipale, J. (2017). Inhibition
948   of p53 improves CRISPR/Cas -mediated precision genome editing Main text.

949 17. Hart, T., and Moffat, J. (2016). BAGEL: A computational framework for identifying
950   essential genes from pooled library screens. BMC Bioinformatics.

951 18. Hart, T., Brown, K.R., Sircoulomb, F., Rottapel, R., and Moffat, J. (2014). Measuring
952   error rates in genomic perturbation screens: gold standards for human functional
953   genomics. Mol Syst Biol *10*.

954 19. Hart, T., Chandrashekhar, M., Aregger, M., Durocher, D., Angers, S., Moffat, J., Crispr,
955   H., Hart, T., Chandrashekhar, M., Aregger, M., et al. (2015). High-Resolution CRISPR
956   Screens Reveal Fitness Genes and Genotype-Specific Cancer Liabilities Screens
957   Reveal Fitness Genes. Cell 1–12.

958 20. Hebbar, N., Wang, C., and Rangnekar, V.M. (2012). Mechanisms of apoptosis by the
959   tumor suppressor Par-4. J. Cell. Physiol. *227*, 3715–3721.

960 21. Hough, S.R., Clements, I., Welch, P.J., and Wiederholt, K.A. (2006). Differentiation of
961   Mouse Embryonic Stem Cells after RNA Interference-Mediated Silencing of OCT4 and
962   Nanog. Stem Cells *24*, 1467–1475.

963 22. Ihry, R.J., Worringer, K.A., Salick, M.R., Frias, E., Ho, D., Kommineni, S., Chen, J.,

964   Sondey, M., Ye, C., Randhawa, R., et al. (2018). p53 inhibits CRISPR/CAS9 engineering
965   in human pluripotent stem cells. Nat. Med. In Press

966 23. Jinek, M., Chylinski, K., Fonfara, I., Hauer, M., Doudna, J.A., and Charpentier, E. (2012).
967   A Programmable Dual-RNA – Guided DNA Endonuclease in Adaptice Bacterial
968   Immunity. Science *337*, 816–822.

969 24. Johnstone, R.W., See, R.H., Sells, S.F., Wang, J., Muthukkumar, S., Englert, C., Haber,
970   D.A., Licht, J.D., Sugrue, S.P., Roberts, T., et al. (1996). A novel repressor, par-4,
971   modulates transcription and growth suppression functions of the Wilms' tumor
972   suppressor WT1. Mol. Cell. Biol. *16*, 6945–6956.

973 25. Kampmann, M., Horlbeck, M.A., Chen, Y., Tsai, J.C., Bassik, M.C., Gilbert, L.A., Villalta,
974   J.E., Kwon, S.C., Chang, H., Kim, V.N., et al. (2015). Next-generation libraries for robust
975   RNA interference-based genome-wide screens. Proc. Natl. Acad. Sci. *112*, E3384–
976   E3391.

977 26. Khandanpour, C., Phelan, J.D., Vassen, L., Schütte, J., Chen, R., Horman, S.R.,
978   Gaudreau, M.C., Krongold, J., Zhu, J., Paul, W.E., et al. (2013). Growth Factor
979   Independence 1 Antagonizes a p53-Induced DNA Damage Response Pathway in
980   Lymphoblastic Leukemia. Cancer Cell *23*, 200–214.

981 27. Kidder, B.L., Hu, G., Yu, Z.-X., Liu, C., and Zhao, K. (2013). Extended Self-Renewal and
982   Accelerated Reprogramming in the Absence of Kdm5b. Mol. Cell. Biol. *33*, 4793–4810.

983 28. Kim, H., Rafiuddin-Shah, M., Tu, H.C., Jeffers, J.R., Zambetti, G.P., Hsieh, J.J.D., and
984   Cheng, E.H.Y. (2006). Hierarchical regulation of mitochondrion-dependent apoptosis by
985   BCL-2 subfamilies. Nat. Cell Biol. *8*, 1348–1358.

986 29. King, H.W., and Klose, R.J. (2017). The pioneer factor OCT4 requires the chromatin
987   remodeller BRG1 to support gene regulatory element function in mouse embryonic stem
988   cells. Elife *6*, 1–24.

989 30. Koike-Yusa, H., Li, Y., Tan, E.P., Velasco-Herrera, M.D.C., and Yusa, K. (2014).
990   Genome-wide recessive genetic screening in mammalian cells with a lentiviral CRISPR-
991   guide RNA library. Nat. Biotechnol. *32*, 267–273.

992 31. König, R., Chiang, C., Tu, B.P., Yan, S.F., DeJesus, P.D., Romero, A., Bergauer, T.,
993   Orth, A., Krueger, U., Zhou, Y., et al. (2007). A probability-based approach for the
994   analysis of large-scale RNAi screens. Nat. Methods *4*, 847–849.

995 32. Kono, K., Tamashiro, D.A.A., and Alarcon, V.B. (2014). Inhibition of RHO-ROCK
996   signaling enhances ICM and suppresses TE characteristics through activation of Hippo
997   signaling in the mouse blastocyst. Dev. Biol.

33. Laurent, L.C., Ulitsky, I., Slavin, I., Tran, H., Schork, A., Morey, R., Lynch, C., Harness, J. V., Lee, S., Barrero, M.J., et al. (2011). Dynamic changes in the copy number of pluripotency and cell proliferation genes in human ESCs and iPSCs during reprogramming and time in culture. Cell Stem Cell *8*, 106–118.

34. Mali, P., Yang, L., Esvelt, K.M., Aach, J., Guell, M., DiCarlo, J.E., Norville, J.E., Church, G.M., Wiedenheft, B., Sternberg, S.H., et al. (2013). RNA-guided human genome engineering via Cas9. Science *339*, 823–826.

35. Mallon, B.S., Chenoweth, J.G., Johnson, K.R., Hamilton, R.S., Tesar, P.J., Yavatkar, A.S., Tyson, L.J., Park, K., Chen, K.G., Fann, Y.C., et al. (2013). StemCellDB: The Human Pluripotent Stem Cell Database at the National Institutes of Health. Stem Cell Res. *10*, 57–66.

36. Masui, S., Nakatake, Y., Toyooka, Y., Shimosato, D., Yagi, R., Takahashi, K., Okochi, H., Okuda, A., Matoba, R., Sharov, A.A., et al. (2007). Pluripotency governed by Sox2 via regulation of Oct3 / 4 expression in mouse embryonic stem cells. Nat. Cell Biol. *9*, 625–635.

37. McDonald, E.R., de Weck, A., Schlabach, M.R., Billy, E., Mavrakis, K.J., Hoffman, G.R., Belur, D., Castelletti, D., Frias, E., Gampa, K., et al. (2017). Project DRIVE: A Compendium of Cancer Dependencies and Synthetic Lethal Relationships Uncovered by Large-Scale, Deep RNAi Screening. Cell *170*, 577–592.e10.

38. Merkle, F.T., Neuhausser, W.M., Santos, D., Valen, E., Gagnon, J.A., Maas, K., Sandoe, J., Schier, A.F., and Eggan, K. (2015). Efficient CRISPR-Cas9-Mediated Generation of Knockin Human Pluripotent Stem Cells Lacking Undesired Mutations at the Targeted Locus. Cell Rep. *11*, 875–883.

39. Merkle, F.T., Ghosh, S., Kamitaki, N., Mitchell, J., Avior, Y., Mello, C., Kashin, S., Mekhoubad, S., Ilic, D., Charlton, M., et al. (2017). Human pluripotent stem cells recurrently acquire and expand dominant negative P53 mutations. Nature 1–11.

40. Meyers, R.M., Bryan, J.G., McFarland, J.M., Weir, B.A., Sizemore, A.E., Xu, H., Dharia, N. V., Montgomery, P.G., Cowley, G.S., Pantel, S., et al. (2017). Computational correction of copy number effect improves specificity of CRISPR-Cas9 essentiality screens in cancer cells. Nat. Genet. *49*, 1779–1784.

41. Munoz, D.M., Cassiani, P.J., Li, L., Billy, E., Korn, J.M., Jones, M.D., Golji, J., Ruddy, D.A., Yu, K., McAllister, G., et al. (2016). CRISPR screens provide a comprehensive assessment of cancer vulnerabilities but generate false-positive hits for highly amplified genomic regions. Cancer Discov.

1032 42. Nichols, J., Zevnik, B., Anastassiadis, K., Niwa, H., Klewe-Nebenius, D., Chambers, I.,
1033   Scholer, H., and Smith, A. (1998). Formation of pluripotent stem cells in the mammalian
1034   embryo dependes on the POU transcription factor Oct4. Cell *95*, 379–391.

1035 43. Ohgushi, M., Matsumura, M., Eiraku, M., Murakami, K., Aramaki, T., Nishiyama, A.,
1036   Muguruma, K., Nakano, T., Suga, H., Ueno, M., et al. (2010). Molecular pathway and
1037   cell state responsible for dissociation-induced apoptosis in human pluripotent stem cells.
1038   Cell Stem Cell *7*, 225–239.

1039 44. Perciavalle, R.M., Stewart, D.P., Koss, B., Lynch, J., Milasta, S., Bathina, M., Temirov,
1040   J., Cleland, M.M., Pelletier, S., Schuetz, J.D., et al. (2012). Anti-apoptotic MCL-1
1041   localizes to the mitochondrial matrix and couples mitochondrial fusionÂ to respiration.
1042   Nat. Cell Biol. *14*, 575–583.

1043 45. Ploner, C., Kofler, R., and Villunger, a (2008). Noxa: at the tip of the balance between
1044   life and death. Oncogene *27*, S84–S92.

1045 46. Qi, L.S., Larson, M.H., Gilbert, L. a, Doudna, J. a, Weissman, J.S., Arkin, A.P., and Lim,
1046   W. a (2013). Repurposing CRISPR as an RNA-guided platform for sequence-specific
1047   control of gene expression. Cell *152*, 1173–1183.

1048 47. Shalem, O., Sanjana, N.E., Hartenian, E., Shi, X., Scott, D. a, Mikkelsen, T.S., Heckl, D.,
1049   Ebert, B.L., Root, D.E., Doench, J.G., et al. (2014). Genome-scale CRISPR-Cas9
1050   knockout screening in human cells. Science *343*, 84–87.

1051 48. Singhal, N., Graumann, J., Wu, G., Araúzo-Bravo, M.J., Han, D.W., Greber, B., Gentile,
1052   L., Mann, M., and Schöler, H.R. (2010). Chromatin-remodeling components of the baf
1053   complex facilitate reprogramming. Cell *141*, 943–955.

1054 49. Sokol, S.Y. (2011). Maintaining embryonic stem cell pluripotency with Wnt signaling.
1055   Development *138*, 4341–4350.

1056 50. Sun, Y., Paşca, S.P., Portmann, T., Goold, C., Worringer, K.A., Guan, W., Chan, K.C.,
1057   Gai, H., Vogt, D., Chen, Y.J.J., et al. (2016). A deleterious Nav1.1 mutation selectively
1058   impairs telencephalic inhibitory neurons derived from Dravet Syndrome patients. Elife *5*,
1059   1–26.

1060 51. Takahashi, K., and Yamanaka, S. (2006). Induction of Pluripotent Stem Cells from
1061   Mouse Embryonic and Adult Fibroblast Cultures by Defined Factors. Cell *126*, 663–676.

1062 52. Takahashi, K., Tanabe, K., Ohnuki, M., Narita, M., Ichisaka, T., Tomoda, K., and
1063   Yamanaka, S. (2007). Induction of Pluripotent Stem Cells from Adult Human Fibroblasts
1064   by Defined Factors. Cell *131*, 861–872.

1065 53. Takashima, Y., Guo, G., Loos, R., Nichols, J., Ficz, G., Krueger, F., Oxley, D., Santos,

1066 F., Clarke, J., Mansfield, W., et al. (2015). Erratum: Resetting Transcription Factor
1067 Control Circuitry toward Ground-State Pluripotency in Human (Cell (2014) 158 (1254-
1068 1269)). Cell *162*, 452–453.

1069 54. Vetterkind, S., and Morgan, K.G. (2009). The pro-apoptotic protein Par-4 facilitates
1070 vascular contractility by cytoskeletal targeting of ZIPK. J. Cell. Mol. Med. *13*, 887–895.

1071 55. Wang, T., Birsoy, K., Hughes, N.W., Krupczak, M., Post, Y., Wei, J.J., Eric, S., and
1072 Sabatini, D.M. (2015). Identification and characterization of essential genes in the
1073 human genome. *13*, 1–10.

1074 56. Wang, W.P., Tzeng, T.Y., Wang, J.Y., Lee, D.C., Lin, Y.H., Wu, P.C., Chen, Y.P., Chiu,
1075 I.M., and Chi, Y.H. (2012). The EP300, KDM5A, KDM6A and KDM6B Chromatin
1076 Regulators Cooperate with KLF4 in the Transcriptional Activation of POU5F1. PLoS One
1077 *7*.

1078 57. Watanabe, K., Ueno, M., Kamiya, D., Nishiyama, A., Matsumura, M., Wataya, T.,
1079 Takahashi, J.B., Nishikawa, S., Nishikawa, S.I., Muguruma, K., et al. (2007). A ROCK
1080 inhibitor permits survival of dissociated human embryonic stem cells. Nat. Biotechnol.
1081 *25*, 681–686.

1082 58. Yamanaka, S. (2000). Essential role of NAT1/p97/DAP5 in embryonic differentiation and
1083 the retinoic acid pathway. EMBO J. *19*, 5533–5541.

1084 59. Yu, J., Vodyanik, M., Smuga-Otto, K., Antosiewicz-Bourget, J., Frane, J.L., Tian, S., Nie,
1085 J., Jonsdottir, G. a, Ruotti, V., Stewart, R., et al. (2007). Induced pluripotent stem cell
1086 lines derived from human somatic cells. Science (80-.). *318*, 1917–1920.

1087 60. Zhang, Y., Schulz, V.P., Reed, B.D., Wang, Z., Pan, X., Mariani, J., Euskirchen, G.,
1088 Snyder, M.P., Vaccarino, F.M., Ivanova, N., et al. (2013). Functional genomic screen of
1089 human stem cell differentiation reveals pathways involved in neurodevelopment and
1090 neurodegeneration. Proc. Natl. Acad. Sci. U. S. A. *110*, 12361–12366.

1091 61. Zhao, M., Kim, P., Mitra, R., Zhao, J., and Zhao, Z. (2016). TSGene 2.0: An updated
1092 literature-based knowledgebase for Tumor Suppressor Genes. Nucleic Acids Res. *44*,
1093 D1023–D1031.

1094

1095